THE UNIVERSITY OF ALBERTA

FIELD ION MICROSCOPY OF ION

BOMBARDED TUNGSTEN

by

© BERNARD GREGOV

A THESIS

SUBMITTED TO THE FACULTY OF GRADUATE STUDIES

IN PARTIAL FULFILMENT OF THE REQUIREMENTS FOR THE DEGREE

OF MASTER OF SCIENCE

DEPARTMENT OF ELECTRICAL ENGINEERING

EDMONTON, ALBERTA

FALL, 1971

UNIVERSITY OF ALBERTA

FACULTY OF GRADUATE STUDIES

The undersigned certify that they have read, and recommend to the Faculty of Graduate Studies for acceptance, a thesis entitled FIELD ION MICROSCOPY OF ION BOMBARDED TUNGSTEN submitted by Bernard Gregov in partial fulfilment of the requirements for the degree of Master of Science.

Date . 4th . June . 1971

ABSTRACT

A bakeable UHV field ion microscope has been constructed to investigate interactions of energetic particles with the surfaces of various materials. The low background pressure in the 10^{-11} torr range allows the irradiation of the target to be performed with the high voltage off. Surface contamination is minimised and the specimen is not under the high field stress during the bombardment time. Energetic gas ions are generated by an ion gun incorporated into the system.

An investigation of the interaction of Ar^+ ions of 150 up to 450 eV energy with tungsten targets has been carried out. Various types of damage such as interstitials, vacancies, and their clusters have been observed on the surface. Annealing of the specimen from solid to liquid nitrogen temperatures caused diffusion of atoms to the surface indicating damage that had been induced in the interior of the tip. More damage has been found on the side of the tip towards the ion source and at higher ion energies the density of damage was increased.

ACKNOWLEDGMENT

TABLE OF CONTENTS

LIST OF FIGURES

LIST OF TABLES

CHAPTER 1

INTRODUCTION

Point defects are the simplest crystal irregularities of atomic dimensions. These imperfections play a great role in the atomic interpretation of many physical properties and processes in solids. For example, point defects play an important role in the understanding of semiconductors since their electrical properties like the electrical conductivity depend on the extent and nature of the impurity defects they contain.

By the controlled production of defects the interpretation of their formation and recovery is facilitated and also the study of their influence on physical properties becomes more exactly determined. A large number of defects can be introduced in a controlled manner into a crystal by irradiation with energetic particles. The radiation damage causes atomic displacements and production of defects in the lattice, introducing changes in the properties of the bombarded solid. The observable changes in the macroscopic properties of the surface and interior have been extensively studied in recent years: namely, changes in thermal and electrical conductivity or changes in optical and mechanical properties were observed[1,2,3].

The technique of field ion microscopy introduced by Muller[4] in 1951, has the distinct advantage over other techniques in that it is able to record directly at atomic resolution the damage resulting from energetic particles. Point defects such as vacancies, inter-

stitials, and their clusters may be resolved. Larger lattice imperfec-
tions such as dislocations and other more complex faults are even more
easily seen. By removing successive atom layers from the surface by
the process of field evaporation the interior of the material can be
studied.

An UHV field ion microscope has been constructed to study
the interaction of energetic particles in the low energy range with
the surface of materials that can be observed in a field ion micro-
scope. The ion gun that has been designed is capable of providing the
bombarding ions of various ion masses in the low energy range. In-
situ specimen preparation is provided with both a tip heater and an
electric pulser that have been built into the system. The former may
be used with a high voltage of up to 15 kV applied to the specimen.
Using the pulser, an atomically clean surface of the tip can be obtained
and by successive field evaporation the interior of the target may be
investigated.

In establishing an experimental correlation among various
parameters of the system a further step has been undertaken to use its
capabilities in investigating the impact of energetic particles on the
solid surface.

Tungsten specimens have been used as targets. Tungsten is
stable at the 450 MV/cm electric field, required for helium ionization;
it can withstand a high field stress and tips are relatively easy to
prepare with the desired low radii.

Inert ions have been conventionally used as the damage species
because of their nonchemical interaction with atoms of the bombarded
solid. Ar^+ ions have been used throughout the course of the present

experiments.   Argon ions with their intermediate mass in the inert gas spectrum, have been thought to be a good choice as damage species in the investigations of the irradiation induced defects using the field ion microscope.   The experiments have been carried out in the energy range from 150 eV to 450 eV.

CHAPTER 2

ION BOMBARDMENT KINETICS

2.1 Radiation damage

Ion bombardment of the surface layers of a solid can be
approximated to radiation damage occurring when more deeply penetrat-
ing particles interact with the bulk of a target. Such damage events
have been and are being well documented[1,2,3].

It is useful to summarize such damage events here, bearing
in mind that ion bombardment events at energies below 10 keV occur
within 100 atomic layers of the surface and are necessarily localized.

In radiation damage the primary knock-on is produced by
interaction with an incident particle. The primary knock-on starts
from a lattice site inside the crystal and slows down to rest either
at an interstitial site (Figure 2.1) or at an atomic site, replacing
a lattice atom. By collisions with other atoms of the lattice the
primary knock-on can produce secondary particles (indicated by dashed
lines in Figure 2.1) with enough energy to escape their lattice sites
and leave a vacancy behind. The secondaries also slow down and come
to rest, either interstitially or substitutionally. In this way a
cascade is produced which eventually consists of n Frenkel pairs and
n interstitials. The number and the positions of the defects depend
on both the magnitude and direction of the primary velocity, the dis-
tribution of which is given by the irradiation conditions. The inter-
action between vacancies and interstitials present in the cascade may
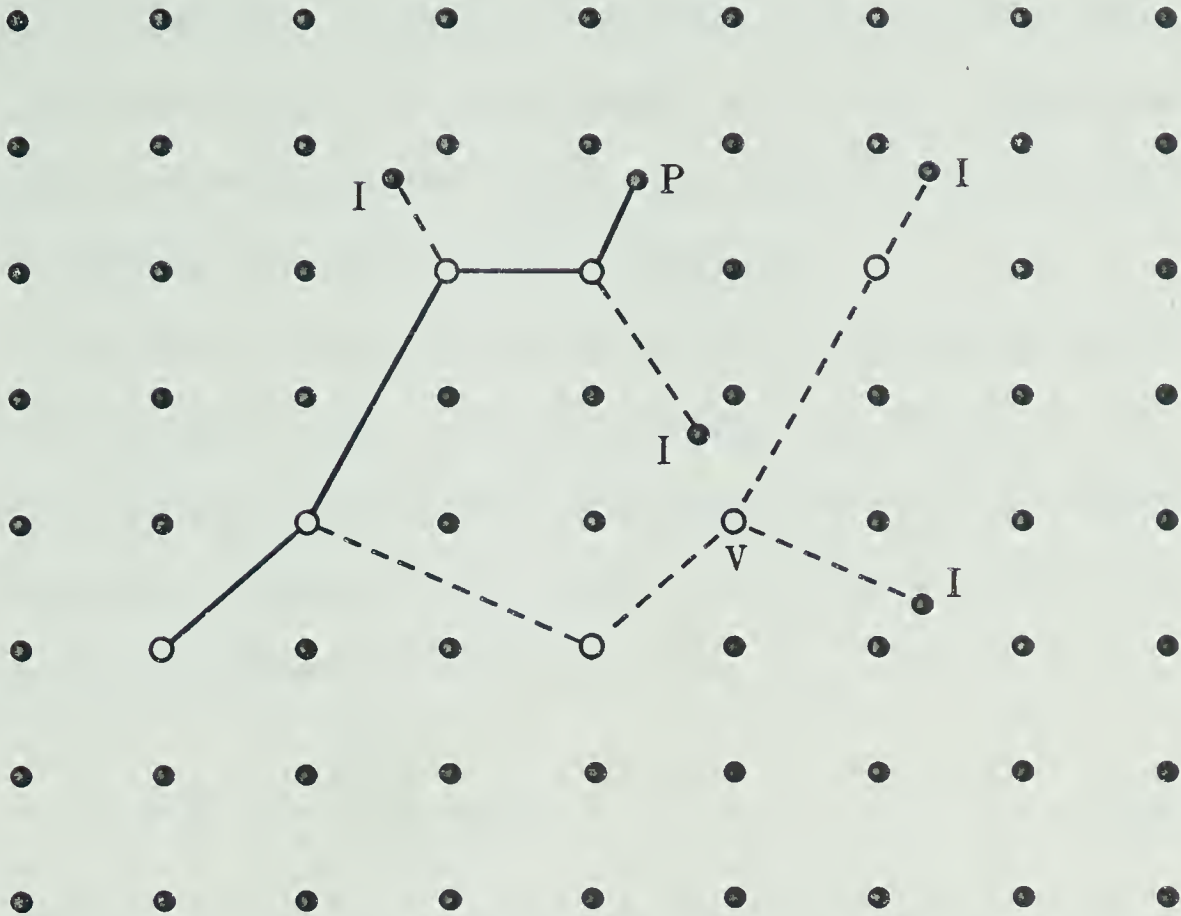
Figure 2.1
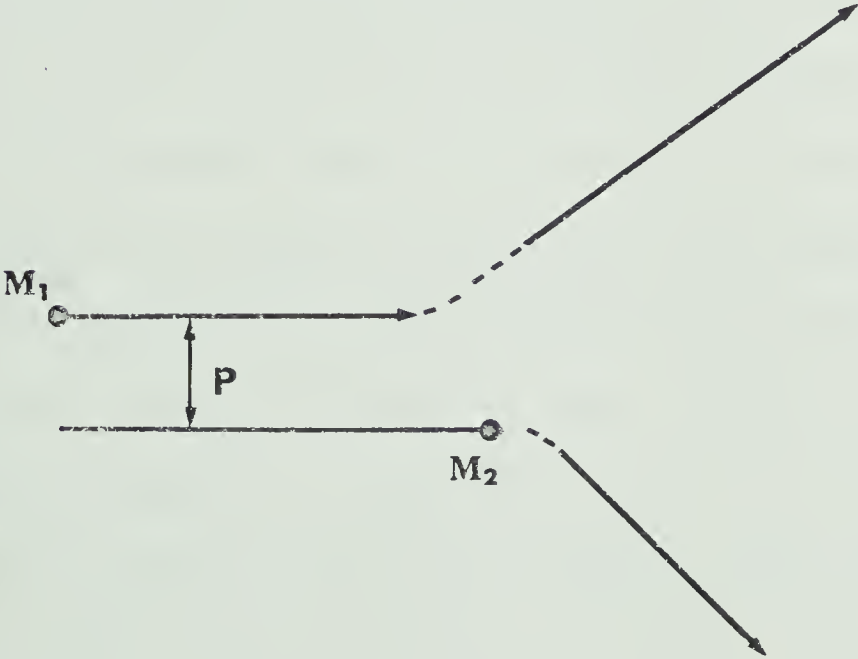
Figure 2.2

lead to the annihilation of one or more Frenkel pairs if the inter-
stitials and the vacancies are close enough. At higher temperatures,
interstitials and vacancies are mobile, thus further thermal anneal-
ing due to diffusive motion has to be considered.

The angle of deflection after collision between an incident
particle of velocity v and a stationary target atom depends on the
energy of the moving particle and on the impact parameter p (Figure
2.2). The energy transfer T ranges from the maximum when the two
particles collide head-on (p = 0) and

$$T = T_m = \frac{4M_1M_2}{(M_1 + M_2)^2} E \tag{2.1}$$

to T = 0 for a glancing collision when p is large.

The collisions which the moving particle experiences can
be divided into two categories: elastic and inelastic. Inelastic
collisions are assumed at higher energies and the major loss of energy
is due to the electronic excitation and ionization of the target atom.
The interaction force is the Coulomb force between nuclear and elect-
ronic charges, the incident primary being ionized to some extend at
high energies due to low velocity orbital electrons having been strip-
ped away. As the particle slows down electrons are collected and the
effective positive charge is reduced to zero. Elastic collisions then
predominate and are similar to those which would occur between hard
spheres. For small energy primaries the lattice imposes rigid condi-
tions upon the possible modes of momentum transfer. When a struck atom
cannot penetrate the surrounding lattice it can only transfer energy

and momentum to one of its immediate neighbours, and so the possibility

of collision correlation becomes apparent. Where close packed rows

of atoms exist in the crystal a sequence of collisions called focusing

may be initiated by an energy pulse. The bundle of energy which passes

down the row is called a focuson. Another possible mode of energy and

mass transfer that may occur is assisted focusing. This collision

sequence occurs when an atom passes through a ring of four atoms and

makes a head-on collision with another atom. For bcc tungsten focus-

ing can occur along the close-packed [111] direction, and assisted

focusing along the [100] direction.

Energetic atoms may move long distances near the central

axes of adjacent rows of atoms which are relatively devoid of inter-

atomic force; this event is called channeling. The mass that trans-

fers down the row is called channelon.

Possible mechanisms for focusing and assisted focusing in

the bcc metals have been studied by Nelson[5]. The interaction between

atoms is described by a Born-Mayer repulsion potential of the form:

$$V(r) = A \exp\left(-\frac{r}{a}\right) \qquad (2.2)$$

Using the empirical constants A and a, Nelson has evaluated values

for the focusing energy E_f^{hkl}, the fractional energy loss per collision

at the focusing energy ε_f^{hkl}, and the number of collisions that a

sequence starting at E_f^{hkl} can travel n_f^{hkl}.

A collective interaction event known as a displacement spike

and thermal spike may occur in the low energy range. The first event

occurs for primary energies of several hundred electron volts. At

these energies the distance between successive collisions is of the order of the interatomic distance so that the primary acts with several lattice atoms almost simultaneously. As a result a multiple vacancy of n lattice sites surrounded by n single interstitials may be caused. When the energy of the primary atom falls below the displacement energy E_d, unable to generate further displacements it dissipates its energy by vibrating at a high frequency and high amplitude transferring energy to the neighbouring lattice atoms. These also oscillate and effectively raise the lattice temperature. This event is known as a thermal spike.

2.2 The transition to the surface

Rapidly developed ultrahigh vacuum techniques and surface preparation have contributed to the increased interest of gas-solid interactions in various fields such as plasma physics, sputtering corrosion of the surface of a space capsule, deposition of thin films, etc. This led to extensive investigations of numerous gas-solid phenomena, such as sputtering, thermal accommodation of gas particles on surfaces, surface ionization and others.

In investigating the interactions of the energetic particles, in both the low and high energy range, with a surface, tungsten has been used as a target by numerous workers. The entrapment of bombarding particles has been studied by Kornelsen[6]. He found that the maximum trapped particle density depends strongly on the ion energy. Kornelsen and Sinha[7,7a] studied thermal release of inert gases from (100), (211), and (110) tungsten surfaces after low energy bombardment. From the number of desorption peaks they suggest that at least five

(Ne) or six (Ar, Kr, Xe) characteristic energies of binding exist. Further, they found strong dependence of the binding energies, corresponding to the desorption peaks, on the crystal face bombarded. Kornelsen et al.[8] have measured a mean 'range' of penetration for 500 eV energy Kr^+ and Xe^+ of the (110) and (211) faces in tungsten. More than 99% of the trapped gas was removed from the crystals when about 10 A° thick layer was taken from its surface. Ion bombardment induced resistivity changes in thin films of polycrystalline Ag, Au, Ti, and W have been studied by Navinsek and Carter[9]. A decrease in resistivity at low ion doses has been interpreted as a result of removal of contaminant gas from the surface. An increase in resistivity at higher ion doses has been attributed to damage production at and near the film surface, and at even higher ion doses the infinite resistivity as a result of sputtering. The increase in the work function of polycrystalline tungsten upon low energy ion bombardment has been observed by Lawson[10]. Annealing caused the work function to fall but either damage or gas desorption may have been the reason for the induced increase in the work function. All these methods among others are indirect in stating the nature of damage that might have been responsible for changes in certain physical properties or processes in the irradiated material.

The capability of the field ion microscope to observe the crystal lattice in atomic detail prompted various workers to use it as a tool to investigate the irradiation induced defects in both the low and high energy range. Undesired contamination of the surface during the irradiation time is removed in the field ion microscope with the high electric field applied to the specimen when working with

helium as an imaging gas[11]. The ionization potentials of the common

contaminants are well below those of helium (ionization potential

24.6 eV) and as a consequence contaminants are field-ionized in space

before they can reach the specimen surface. This advantage offered

by the field ion microscope has been used by Muller[12] and Brandon

et al.[13] in their investigations of radiation damage. However, the

effect of the field stress which amounts to 9×10^{10} dynes/cm^2 under best

imaging conditions at 450 MV/cm, introduces up to 10% dilatation in

the specimen lattice[14], thus it may affect the nature of the damage

of the surface and in the interior of the specimen. In order to

eliminate the effect of the field stress several authors have used a

UHV microscope so that the high voltage could be turned off during the

bombarding time. A summary of the unpublished work of these authors

is given in reference [15]; Strayer et al. have studied the effect of

the impact of Xe^+ ions on tungsten in the energy range of 100 to

1300 eV. They found that at 100 eV energy most of the damage occurs

at the side of the tip away from the beam, while at 1300 eV the damage

is mostly towards the ion source; further, they found some indication

of Xe atom burial within the first few atom layers of the tip. Using

He^+ ions between 50 and 4000 eV Strayer et al.[15] found the sputtering

events to occur mostly on the beam incident side. Bombarding a tung-

sten tip with the ions produced from a mixture of 90% He and 10% Ar

Wald[15] found a slip on {112} planes toward the beam at energies up to

400 eV. A dislocation loop was traced 20 layers deep. The radiation

damage resulting from 10 MeV protons was observed by Petroff and

Washburn[16] with the high voltage both off and on. More extensive

damage was found on the specimens that were irradiated with the high

field on.

The UHV system described in chapter 4 allows irradiation

with the high voltage turned off providing the bombardment is completed

in a relatively short time. So without the applied field the lattice

is not distorted during the bombardment time.

CHAPTER 3

FUNDAMENTALS OF FIELD ION MICROSCOPY

The field ion microscope (FIM) discovered in 1951 by

E.W. Muller[4] is the only device capable of resolving the individual

atoms of a surface (Figure 3.1). By displaying the atomic structure

of the specimen, the observation of lattice defects is possible. The

FIM microscope is uniquely suitable for the study of point defects

and the results presented in chapter 6 well justify its use as a tool

to investigate irradiation effects on tungsten specimens. This

chapter deals with features of the field ion microscope. Basic prin-

ciples of the field ion microscope as well as field ionization and

field evaporation are described in this chapter. The field ion micro-

scope design and operation are described in chapters 4 and 5.

3.1 Basic principles of the field ion microscope

The specimen in the form of thin wire, which had been elect-

ropolished to an extremely fine point is mounted inside a vacuum

chamber and points at a fluorescent screen (Figure 3.2). In operation

the chamber is first pumped down to a background pressure less than

1×10^{-7} torr. An imaging gas, normally helium, is then introduced into

the chamber to a pressure of about 3×10^{-3} torr. The specimen is con-

nected to the leads that enable a positive electrical potential to be

applied to the specimen. At the same time they serve as a good thermal

conductor to the coolant (liquid nitrogen, hydrogen or helium).
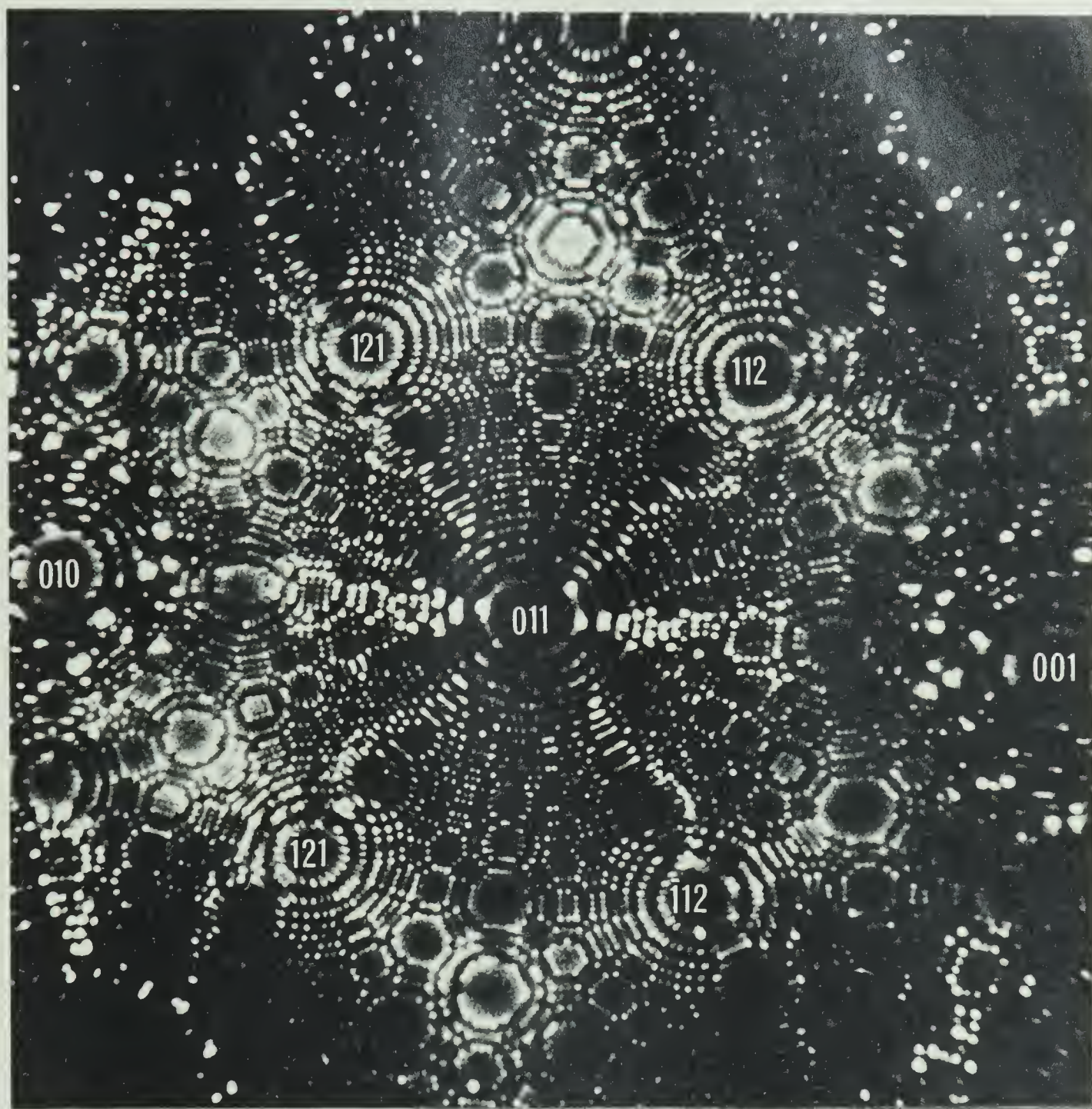
Figure 3.1   Field ion micrograph of a tungsten tip of
approximately 600A radius.   Imaging gas helium
at pressure of 2×10^{-3} torr.   Tip voltage
13,600v.   Exposure time 15 secs using Tri-X-
Pan developed in Diafine.

The high curvature of the tip enables fields of a few hundred MV/cm to be produced by an applied potential of a few kilovolts. The field is strong enough to cause ionization of the atoms of the imaging gas as they are attracted to the tip surface by polarization forces. The generated positive ions are repelled from the tip surface and following approximately radial paths they strike and excite the screen. Each white spot corresponds to an individual atom.

The magnification is approximately equal to the ratio of the tip-screen distance to the tip radius. With a tip-screen distance of 10 cm an image is magnified by one million times with a specimen of 1000 A° radius.

3.2 Field ionization

An electron in an atom in the absence of an external field finds itself in a potential trough[17] as shown in Figure 3.3a. The ionization energy must be added to excite the electron and ionize the atom. Figure 3.3b shows the effect of an applied field; the potential barrier is reduced but even without excitation the ionization can occur if the electron tunnels through the potential barrier along the path AB. When the atom is near the surface of a metal, the potential barrier is further reduced by image forces which attract the electron to the image dipole induced in the metal. Figure 3.3c shows a gas atom at the closest distance at which tunneling can occur with the given field. If the atom moves closer to the surface the electron energy level in the atom falls below the Fermi level in the metal and the tunneling probability is greatly reduced because of the low density of vacant states to which the electron may tunnel. Field

To high voltage
power supply

Coolant

Accelerating shield

Specimen

Ion trajectories

To vacuum pump
and gas supply

Fluorescent screen on
conductive coating
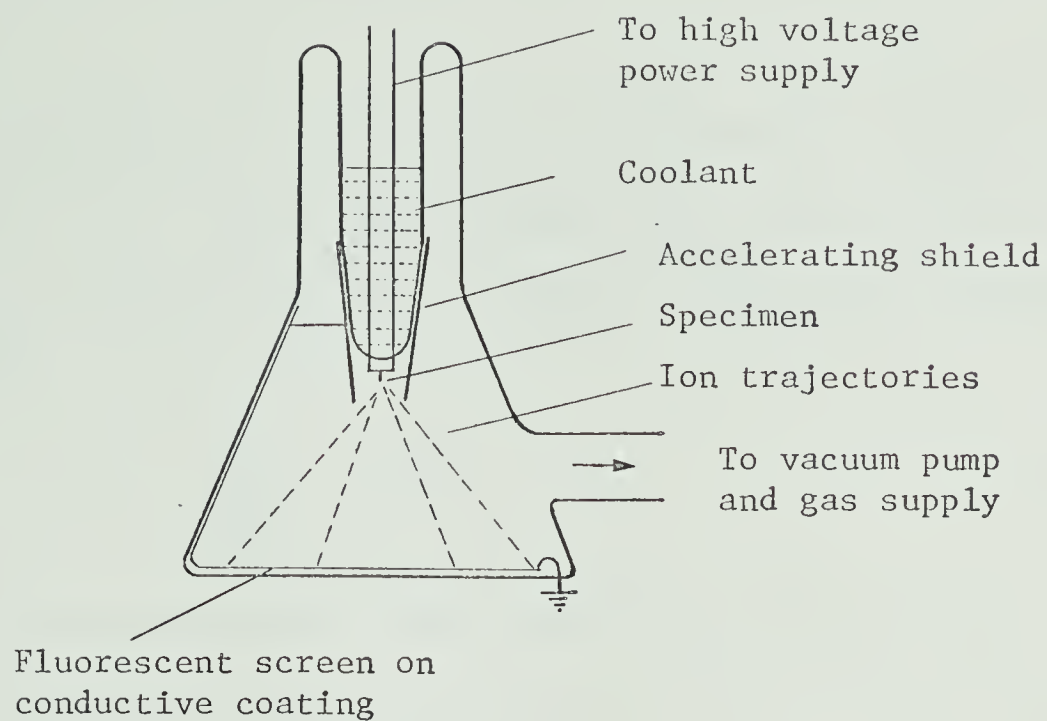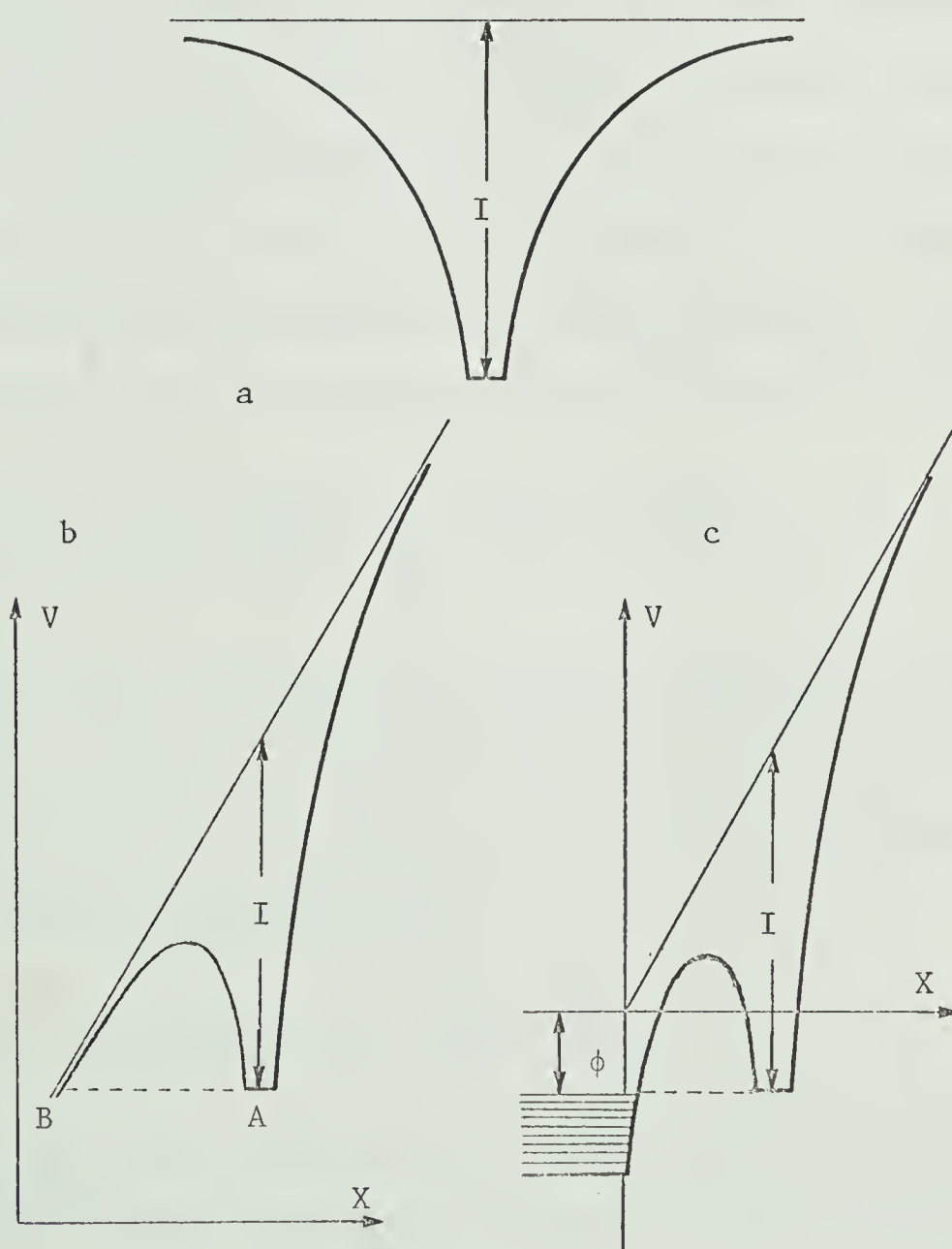
Figure 3.2

Figure 3.3

ionization by tunneling of the electron into the metal therefore cannot occur at $x < x_c$. The critical distance for field ionization, x_c and at the same time the distance of greatest penetration probability, is given by[11]

$$eFx_c = I - \phi - \frac{e^2}{4x_c} + \frac{1}{2} F^2(\alpha_A - \alpha_I) \qquad (3.1)$$

where ϕ is the work function of the metal and α_A and α_I are the polarizabilities of the gas atom and the resultant ion. The third term is the image potential of the electron and the fourth term represents the difference in the polarization energy before and after ionization. The last two terms are very small compared to I and ϕ, thus equation 3.1 can be reduced to $x_c = (I - \phi)/eF$ from which the critical distance $x_c \simeq 4.5$ A° for the case of helium (I = 24.5 eV) ionized above a tungsten surface (ϕ = 4.5 eV) at a field strength of 450 MV/cm.

The penetration probability D for the tunneling electron may be calculated from the WKB approximation[18,19] and is of the form

$$D(E,V(x)) = \exp\{-(\frac{8m}{\hbar^2})^{\frac{1}{2}} \int_{x_1}^{x_2} [V(x) - E]^{\frac{1}{2}}dx\} \qquad (3.2)$$

where $V(x)$ and E are the electron's potential and kinetic energies, m is its mass, $\hbar$ Planck's constant divided by 2π, and x_1 and x_2 denote edges of the barrier at the energy level of E. For $V(x)$ Muller and Bahadur[20] give this approximation.

$$V(x) = -\frac{e^2}{(x_n - x)} + Fex - \frac{e^2}{4x} + \frac{e^2}{x_n + x} \qquad (3.3)$$

in which the first term represents the Coulomb potential due to a positive ion of charge e located at a distance x_n from the plane

surface of the metal. The second term is the potential energy of the electron due to the applied field and the last two terms are image potentials due to the electron and ion images, respectively.

From the theoretical consideration, two characteristics of field ionization are apparent; ionization probability is strongly dependent on the magnitude of the field and the probability increases rapidly toward the tip surface and disappears at the critical distance x_c. The measurements of the energy distributions of field ions[20,21] locate the origin of the ionization and well confirm the existence of the critical ionization distance x_c. The energy distribution of helium ions from a tungsten surface was calculated by Muller and Tsong[21]. They found the distribution half-width at best image field (F = 440 MV/cm) to be about 0.8 eV, which corresponds to a narrow ionization zone of 0.18 A° depth (similar results were obtained for other gases: argon, neon and hydrogen).

3.3 Field ion current

The current-voltage characteristics of the field-ion microscope also give information that support the theory of field ionization. The current-voltage characteristics of a helium-operated field ion microscope with the tip temperature down to 63°K are given by Southon and Brandon[22]. Figure 3.4 shows two distinct linear ranges. The ion current increases initially very sharply with applied voltage with slope of about 30 as could be expected from the strong dependence of the ionization probability on field strength. The relatively slow increase of ion current with field beyond the transition region indicates that the ionization probability has saturated at a value
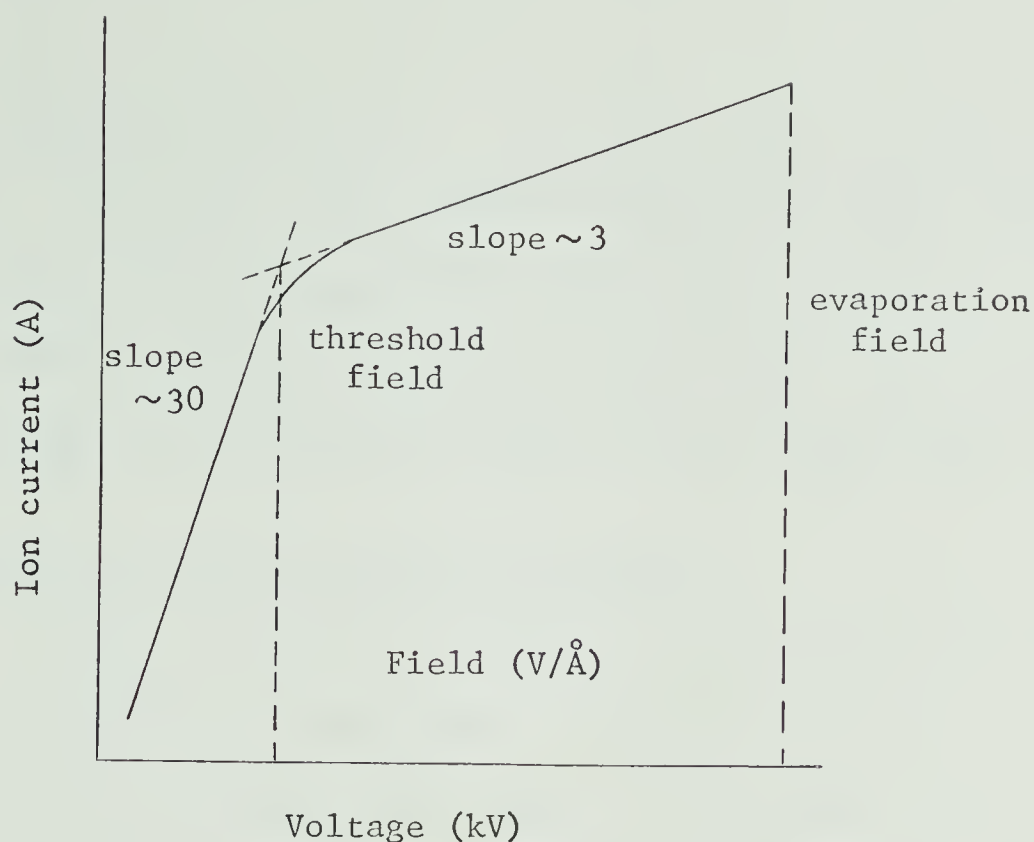
Figure 3.4

corresponding to the certain ionization of any gas atom near the emitter surface but that the supply of gas to the emitting region continues to increase slowly with field strength.

3.4 Gas supply function

Due to the attraction in the inhomogeneous field of polarized gas molecules the gas supply is larger by a factor of 10 to 100 than expected on the basis of simple gas kinetics[17,23]. Calculations of the gas supply by dipole attraction to a sphere of radius r_t, for which the field F at a distance r from the center is $F(r) = (\frac{r_t}{r})^2 F_o$ have been made by various authors[12,22,23]. The potential energy of a gas atom in an electric field F is given by $V(F) = -\mu F - \frac{1}{2} \alpha F^2$ where α is the polarizability and μ is the permanent dipole moment associated with the particle. Upon collision with the tip surface, some of the gas atoms retain sufficient kinetic energy to escape from the polarization potential well. The remaining number transfer some of their

kinetic energy to the lattice. As a result, their rebound energy is too small to let them escape from the high field region around the tip. Trapped by dipole attraction, they continue bouncing over the tip surface until after having been accommodated to the tip temperature in a sequence of up to several hundred contacts they become ionized.

3.5 Resolution of the field ion microscope

Three main factors contribute to the resolution of the field ion microscope[24]. One that takes into account a diffraction limitation due to the de Broglie wavelength of the imaging particle localized within a region Δy_t parallel to the emitter surface has, from the Heisenberg principle, a transverse velocity $v_t = \hbar/2m\Delta y_t$. A second factor is a loss of resolution due to the thermal lateral velocity of the ions, and a third factor would be the one that takes into account the ionization that may occur from any point in a disk of diameter δ_o. For small x_c, the ionization disk diameter is assumed to be of the order of the radius of the image gas molecule.

The resultant resolution is given by

$$\delta = \delta_o + \left\{ 4 \left(\frac{\beta^2 r_t \hbar^2}{2\kappa e M F_o} \right)^{\frac{1}{2}} + 16 \left(\frac{\beta^2 r_t kT}{k e F_o} \right)^{\frac{1}{2}} \right\}^{\frac{1}{2}} \quad (3.4)$$

where β is an image compression factor, and κ is a geometrical factor. The best resolution will be found by working with the smallest possible tip radius r_t, low temperatures and by imaging with a gas with the highest ionization field F_o and smallest atomic radius. Helium, possessing both a small atomic size and the highest ionization potential is the best choice as an imaging gas, for tungsten tips.

3.6 Field evaporation

Tips cleaned by heating still have considerable surface roughness in the form of superficial atoms on top of the completed lattice planes. When the field is increased to the point where field desorption of the lattice itself occurs, perfect surfaces free from thermal disorder can be obtained[23]. The term field evaporation was introduced by Muller to distinguish the process of evaporation of a metal from its own lattice from the process of desorption, i.e. the analogous process for the removal of foreign atoms at the surface. Protruding surface atoms are removed in the form of positive ions. Field enhancement over these atoms reduces the activation energy for field evaporation in these regions, so that protruding atoms at the surface of a field ion microscope tip are evaporated preferentially[11].

Observation of the bulk of the specimen can also be carried out by successive field evaporation of surface layers[23]. Field evaporation was first interpreted by Muller as a thermally activated process when he discovered the phenomenon and suggested the image force theory. Since then a few minor modifications in the activation energy therm have been introduced by various authors[11,17,25]. In their theory of field evaporation, they have shown that partial atomic tunneling can occur. The activation energy with assumption that Q_n is given by the intersection point of ionic and atomic potential curves of the atom and the ion near the metal surface is given by[17,25]

$$Q_n = A + \sum_n I_n - n\phi - \frac{n^2 e^2}{4x_c^{(n)}} - neFx_c^{(n)} + \frac{1}{2}(\alpha_A - \alpha_I^{(n)})F^2 \quad (3.5)$$

where x_c is the distance of the intersection point from the metal

surface, the subscript n denotes the charge of the ions in a unit of

electronic charge e, Λ is the sublimation energy of the surface atom,

I_n the nth ionization energy, F is the electric field on the metal

surface and α_A and $\alpha_I^{(n)}$ the polarizabilities of the atom and the ion

respectively.

The field for evaporation as n-fold charged ions is given

by

$$F_n \approx \frac{1}{ner_o} \left(\Lambda + \sum_n I - n\phi - \frac{n^2 e^2}{4r_o} \right) \tag{3.6}$$

where r_o is one half the nearest neighbors distance of the metal

lattice.

Comparison of the field evaporation fields for singly and

doubly charged ions[17,23,25] shows that for most metals F_2 is consider-

ably lower than F_1, therefore these materials will field evaporate as

doubly charged ions at low temperatures and corresponding fields are

the evaporation fields.

CHAPTER 4

DESIGN OF THE APPARATUS

4.1 Microscope design

As has been mentioned in the previous chapter, the helium
FIM emitter surface is protected from residual gas contamination as
long as the imaging field is on. In the presence of a gas at a
pressure p, a clean surface will soon be covered with an adsorption
layer and after a time of exposure t the degree of coverage of an (hkl)
plane of a bcc lattice is given by[15]

$$\beta_n = \frac{\delta a^2}{2} \left(\frac{h^2 + k^2 + l^2}{2\pi MkT_g} \right)^{\frac{1}{2}} n_{hkl} \, p \, t \tag{4.1}$$

where $\delta = 1$ if $h + k + l$ is even, or $\delta = 2$ if $h + k + l$ is odd, and
n_{hkl} is the sticking coefficient of the gas molecules on the (hkl)
plane. For the experiments described in this thesis, the degree of
contamination must be minimized by the use of ultra-high vacuum
techniques since target bombardment is performed with the imaging
voltage off.

The design of the bakeable, stainless steel microscope well
meets this requirement. The system has proved adequate for back-
ground pressure down to 6×10^{-11} torr at liquid nitrogen temperature.

Figures 4.1 and 4.2 show the design of the microscope chamber.
The microscope chamber has two dewars. The inner glass dewar sealed
to Kovar tubing flanged at the top, is sufficiently well shielded to
allow liquid hydrogen or liquid helium to be employed.

23

inner
dewar

outer
dewar

re-entrant
screen
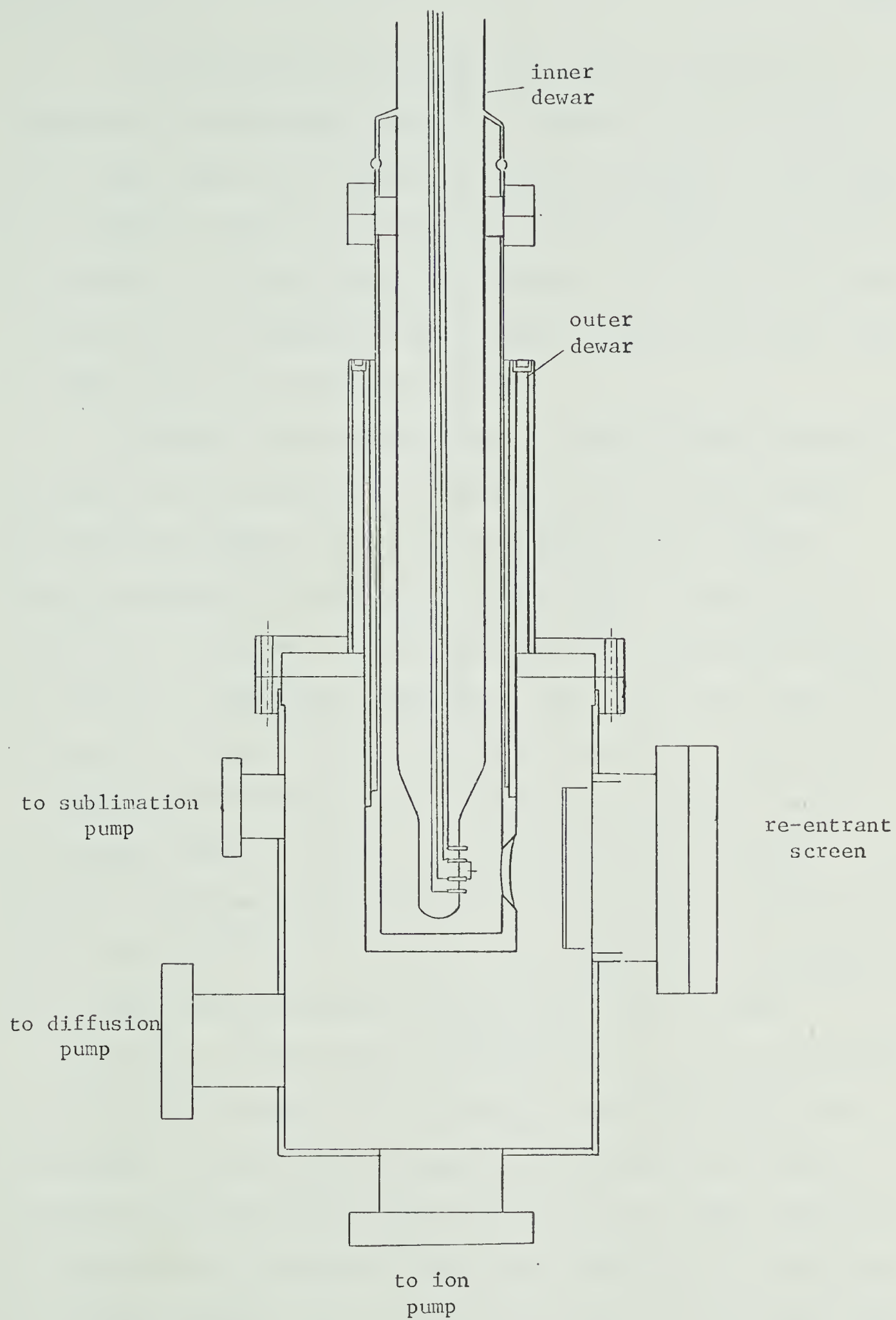
to sublimation
pump

to diffusion
pump

to ion
pump

Figure 4.1

At the bottom of the inner glass dewar four horizontal tungsten wire feedthroughs mounted in a vertical plane are provided. Two of these support the filament to which the specimen is spot welded, and two are to connect the thermocouple to measure the temperature of the specimen. The feedthroughs are connected to the electrical leads of which two go to the heating and the high voltage power supply, and the other two to the temperature monitor.

The four inch diameter reentrant viewing window positioned two inches from the specimen is mounted on a five inch UHV flange. The microscope chamber is connected by a $2\frac{1}{2}$ inch Varian bakeable valve to an Edwards oil-diffusion pump E02, which is backed by an Edwards ED75 rotary pump. These pumps remove the inert gases during the imaging and bombardment experiments. The 3 inch side flange for housing the ion gun assembly is positioned so that its central axis coincides with the tip position. Two 1 inch ports are provided for the pressure measuring devices. One port is used for a Varian MilliTorr ionization gauge which operates in the high pressure range from 1 torr to 10^{-5} torr, and another for a Varian UHV series gauge which gives pressure measurement from 10^{-3} torr down to about 2×10^{-11} torr. An AEI minimass mass spectrometer is also incorporated into the system to monitor the residual gas composition during the experiments. A port, directly opposite the ion gun can be used to irradiate the specimen with a laser beam or for any other purpose in the future. It is at present flanged with a window and has been used to check the position of the specimen with respect to the central axis of the gun and also for gun alignment itself. A one inch diameter

liquid nitrogen
dewar

A

viewing
port

A

pumping line
port

ion pump port

ion gun port

sublimation
pump port

Section A-A

B

B

minimass

millitorr
gauge

low
ionization
gauge

leak port

Section B-B
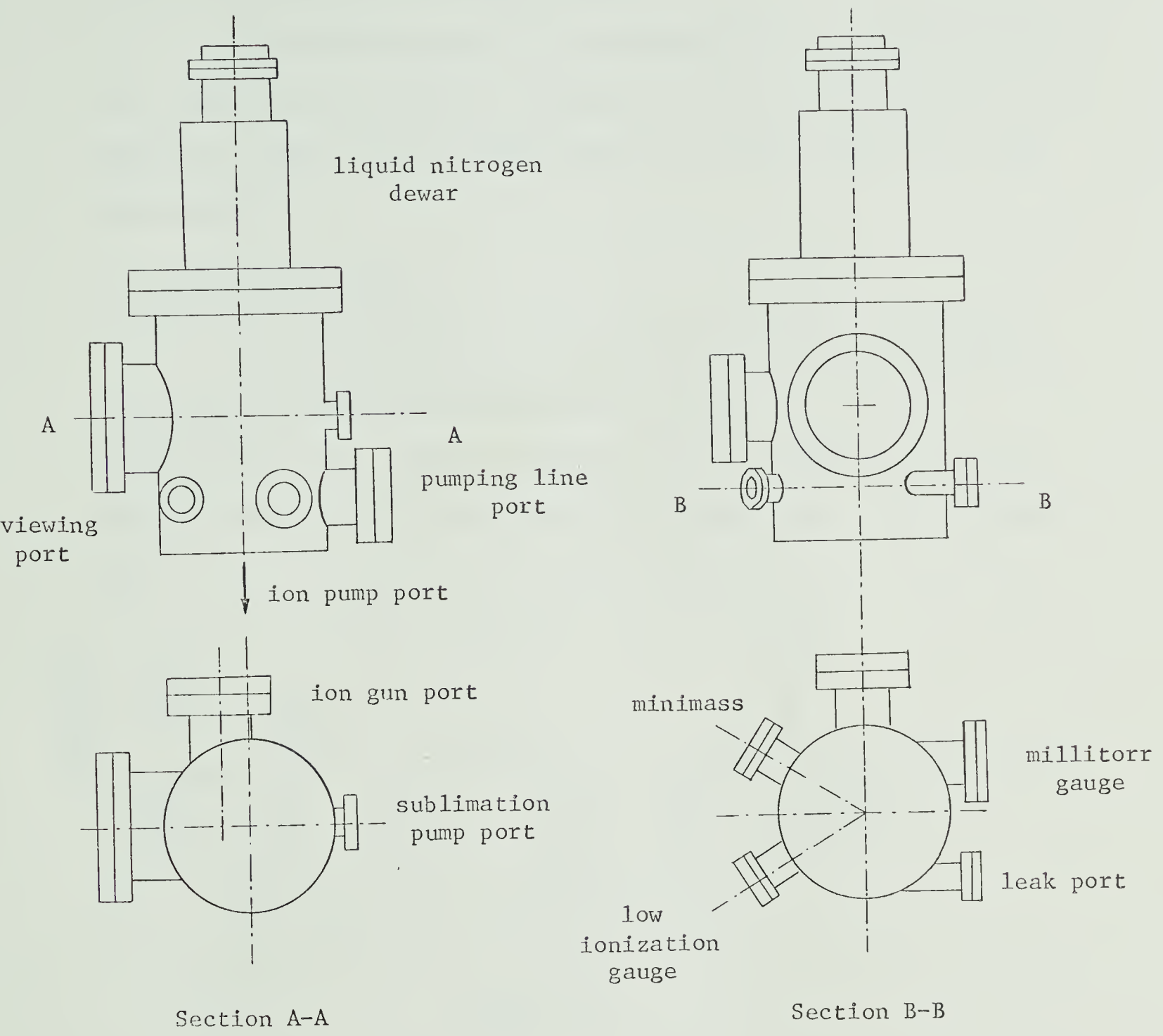
Figure 4.2

port connects the microscope chamber to the gas handling plant through

a bakeable, Varian variable leak valve.

The microscope itself is constructed from type 304 stainless

steel using inert gas welding techniques followed by passivation. All

windows are pyrex and all flange bolts are stainless steel with OFHC

copper gaskets.

4.2 Gas handling plant

Inert gases are introduced into the chamber of the micro-

scope from an unbaked gas handling plant (Figure 4.3) via the

variable leak valve. The gas handling plant is pumped by a mercury

diffusion pump backed by an Edwards ED35 rotary pump. This configura-

tion
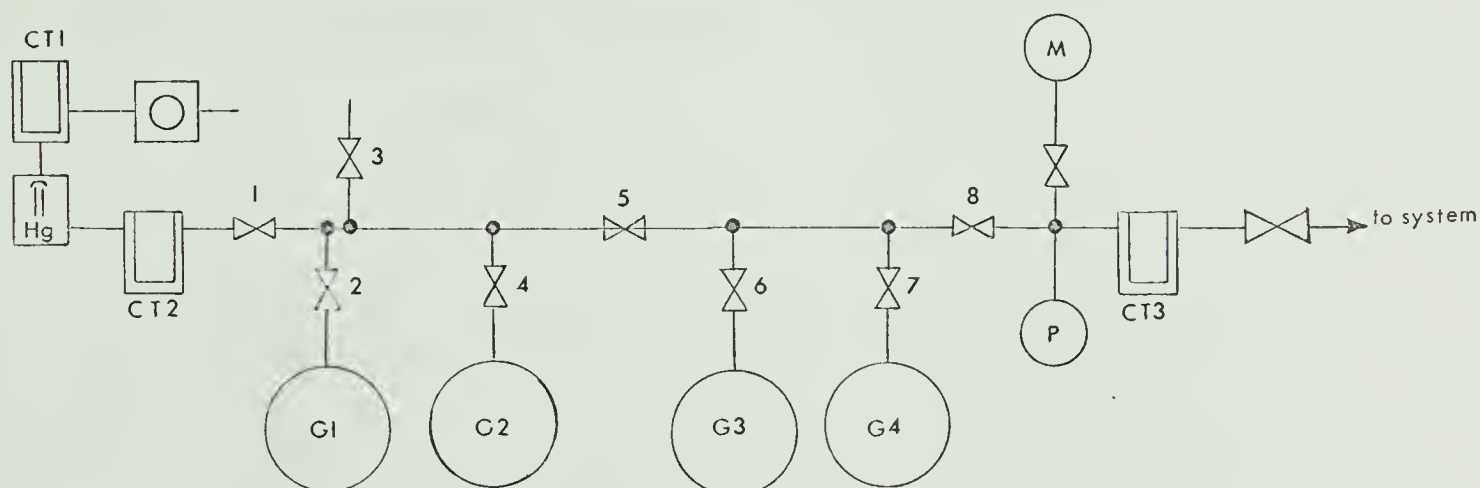
Figure 4.3

was found desirable because of the need to reduce the base pressure

of the GHP, inhibiting the introduction of contaminants into the

inert gas. The cold traps: CTI inserted between the rotary pump and

diffusion pump, CT2 set after the diffusion pump and CT3 in front of

the leak valve are all filled with liquid nitrogen and maintain a

background pressure in the GHP line below 10^{-4} torr. Spectroscopic-

ally pure inert gas is supplied by the Airco Company in 1 litre flasks

and connected to the GHP via glass tubes. Two one litre glass flasks

are used as reservoirs where helium and argon were stored at a

pressure of several torr after being expanded into the GHP line from

the helium and argon flasks respectively. The pressure in the GHP is

measured by a Pirani gauge. A spare line is provided to connect an

Edwards Vacustat gauge that can be used for calibration of the gauges

in the system.

4.3 Ion gun

Low energy positive ions for tip bombardment are generated

in the ion gun shown in Figure 4.4.

Figure 4.4

The basic design of the ion source and ion optics is similar to that

described by Hagstrum[26]. The operation of the apparatus is as follows:

electrons from the filament A are accelerated through apertures in

electrodes B and C and are collected at T. The ions formed by electron

impact inside the chamber C are drawn out through an aperture in F. The ion repeller IR with its small positive potential directs the ions towards the aperture in F. The ion beam is focused by the 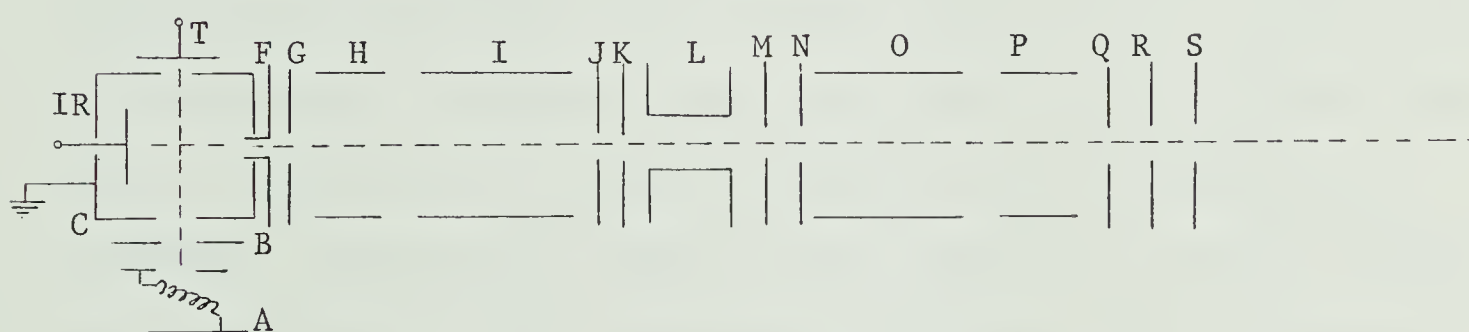system of ion lenses formed by electrodes F through G. The ion energy at the target surface is determined by the negative voltage applied to the specimen.

In table 4.1 typical potentials for electrodes A to S are given for Ar^+ ions, and 250 eV ion energy. The energy spread in the ion beam of 250 eV energy and potentials listed in table 4.1 is 20 eV, measured by applying a retarding potential to the target. The potentials listed in table 4.1 are not unique. For various ion energies one will find it necessary to set different potentials at the electrodes O, P, Q, R, and S to obtain the optimum operational conditions. Here, it should be noted that the alignment of the specimen tip with the central axis of the ion gun is very important.

All electrodes have been made of stainless steel and held in position by being mounted on four alumina rods which pass through holes in the electrodes accurately placed with respect to the electrode apertures. Electrodes are separated by alumina washers of appropriate thickness. The stack thus formed is held together by friction springs which slip directly on the supporting alumina rods. This arrangement has been found to provide good aperture alignment.

The source filament is 0.01 inch diameter thoriated tungsten wire. Dimensions of the apparatus of Figure 4.4 are also given in table 4.1.

Table 4.1

Electrode	Distance from preceding electrode [inches]	Slit diameter [inches]	Potential [volts]
A	0.1	0.24	−80
B	0.1	0.18	−10
C	0.1	0.12	0
F	0.08	0.18	−50
G	0.1	0.24	−20
H	0.1	1.0	−50
I	0.1	1.0	−30
J	0.1	0.12	−130
K	0.14	0.18	−120
L	0.1	0.22	−50
M	0.1	0.12	−70
N	0.14	0.18	−50
O	0.1	1.0	−20
P	0.1	1.0	−30
Q	0.1	0.24	−50
R	0.08	0.24	−65
S	0.08	0.24	−30
T	0.1		+80
IR			+10

CHAPTER 5

EXPERIMENTAL

5.1 Vacuum processing

An ED75 rotary pump pumps the vacuum system down to 10^{-3}
torr and also serves to back a 150 litre/sec oil-diffusion pump which
is trapped by a water-cooled baffle and liquid nitrogen cold traps.
A UHV valve situated between the microscope chamber and the cold trap
serves to valve the chamber. The system is pumped to ultra-high
vacuum by means of the ion pump and titanium sublimation pump. The
diffusion pump is incorporated to handle the high pressure of inert
gases argon and helium. Exposure of the ion pump to high inert gas
pressures leads to previously pumped gases being liberated and to
contamination of the imaging gases.

Since in the operation of the microscope the microscope
chamber is disconnected from the diffusion pump and backfilled with
the imaging gas, a low outgassing rate of the system is of major
importance. A low enough background pressure of the system may be
retained after baking the system out.

The vacuum system was baked at 350°C each time after the
system was exposed to the air when replacing the specimen. Bakeable
parts of the complete system are shown within the dotted line, Figure
5.1. After a new specimen had been inserted into the system it was
inspected for possible faults to avoid unnecessary baking out. During
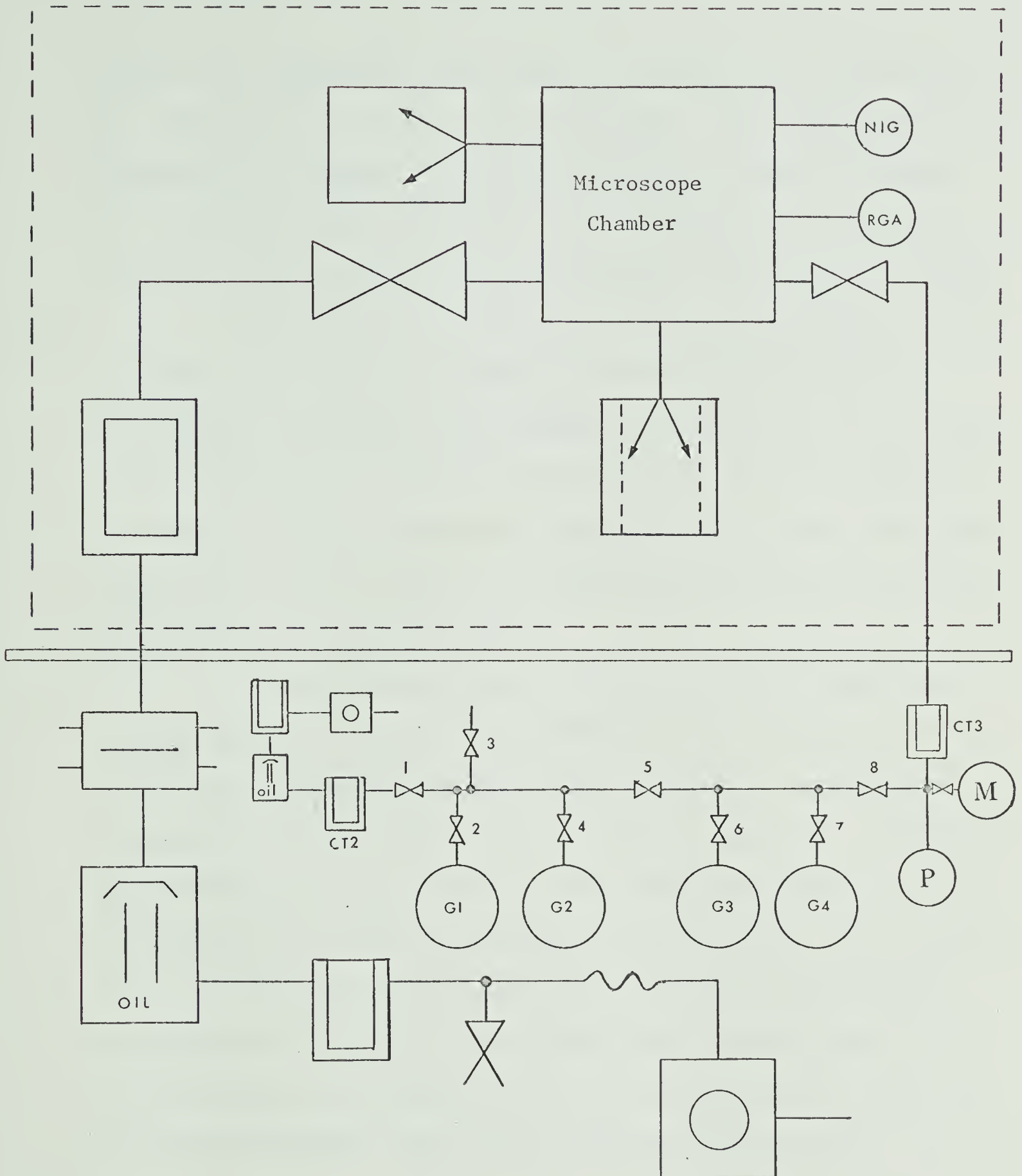the baking out metal filaments were thoroughly outgassed. The ion gun

Figure 5.1

(The symbols conform to American Vacuum
Society Standard AVS7.1-1966)

filament was outgassed by increasing its current by one ampere above the value when the gun is in normal operation. The sublimation pump filaments were outgassed in turn with currents of about 30 amperes as recommended by the manufacturer. The ion gauges were outgassed from their own units where electron bombardment degassing is provided.

The necessity for a clean ultra-high vacuum chamber for the experiments that have been carried out has been mentioned already. The titanium sublimation pump connected to the main body of the microscope (Figure 5.1) very effectively purifies the inert gases (helium and argon). A freshly evaporated titanium film in a getter bulb pumps active gases like CO, CO_2, H_2 etc. very effectively while having zero pumping speed for the inert gases.

Actually, the leak valve was set at a certain leak rate (approximately 10^{-6} lit/sec); when the UHV valve was kept open for one or two turns, maintaining an equilibrium pressure in the system of approximately 2×10^{-3} torr, so the microscope chamber was continuously pumped during the imaging period. This procedure was found to prevent the possibility of impurity accumulation; since the GHP is not bakeable this was thought desirable because one could expect small amount of contaminants in the GHP line regardless of the liquid nitrogen traps in the GHP line. The required cooling of the specimen is carried out with liquid nitrogen, which cools the specimen down to 78°K.

5.2 System calibration

The conductance of the leak valve was established when opening the knob of the leak valve approximately 2 turns. The system equation is:

$$Q - Sp_s = V_s \frac{dp_s}{dt} \tag{5.1}$$

where $Q = k(p_g - p_s)$ in the quantity of the gas flow per second

through the leak valve of conductance k litres/sec.

p_g —   gas handling plant pressure, measured by a vacustat, torr

p_s —   system pressure, torr

Sp_s —   net quantity of gas removed at the bakeable UHV valve of

        pumping speed S litres/sec.

$V_s \frac{dp_s}{dt}$ — net quantity of gas received into the system volume V_s

        litres

The gas balance equation for the GHP may be written as:

$$-kp_g = V_g \frac{dp_g}{dt}$$

since $p_g \gg p_s$, yielding:

$$p_g = p_{g_0} \exp\left(- \frac{k}{V_g} t\right) \tag{5.2}$$

From the graph of $\ln p_g$ versus time t the leak conductance k is

calculated.

      The pumping speed S can be calculated from equation (5.1)

by recording the ion gauge pressure variation with time when the valve

is opened to allow the gas admitted to the system from the GHP, to

pump away. This speed is too high to be accurately measured in this

pump-down method, therefore the speed was reduced by partially opening

the valve and this speed S' is calculated from the equation (5.1):

$$-S'p_s = V_s \frac{dp_s}{dt} \qquad \text{i.e.}$$

$$P_s = P_{so} \exp(-\frac{S'}{V_s} t) \tag{5.3}$$

The system volume was determined from the design data of the system. From the plot of $\ln P_s$ against time t the pumping speed S' has been calculated.

With speed S' maintained the GHP pressure was set up to various values, and when equilibrium was established, readings of the system pressure were taken. Equation $Q - S'p_s = V_s \frac{dp_s}{dt}$ becomes in the steady state $Q = S'p_s = kp_g$, yielding:

$$P_s = \frac{k}{S'} P_g \tag{5.4}$$

and system pressure can be evaluated. The gauge constant has been obtained by plotting p_s observable versus p_s evaluated from equation (5.4). This calibration was carried out for air, helium and argon. The corresponding constants were 0.96, 0.09 and 1.35 respectively.

5.3 Phosphorescent screen

The helium ions are converted into a visible image by allowing the ions to strike a fluorescent screen. The screen glass plate is coated with a conductive layer of tin oxide and welded to the Kovar flange.

The conducting transparent glass was prepared by a technique introduced by Gomer[27]. During the initial construction of the microscope it was felt advisable to mount the glass screen onto a stainless steel flange. Stray magnetic fields could affect the helium ion trajectory before striking the phosphor. However, constructional difficulties, manifested by the window cracking during system bakeout,

precluded this technique and a Kovar tube was eventually used. Mag-
netic aberrations were found to be almost non-existent and the sub-
sequent micrographs were perfectly satisfactory.

The phosphor screen is deposited by sedimentation. The
window is immersed into a vessel containing distilled water. After
the water in the vessel has stabilized a suspension of finely ground
phosphor in water is poured into the vessel and the phosphor is
allowed to settle out. The water is removed by careful siphoning.
The screen is allowed to dry and the window mounted into the system.

Sylvania phosphor, type 161, $Zn_2 SiO_4$:Mn is used. The
deterioration of this phosphor under ion bombardment has been found
to be smaller and therefore was preffered to more efficient phosphor
materials such as ZnS or CdS - ZnS[11]. Muller found that this phosphor
lasts about 10 times longer than the zinc sulfides[28].

5.4 Specimen preparation

The specimen used in a FIM is a needle shaped wire with a
tip radius of usually one to a few hundred angstroms and a shank
angle of 20 to 30 degrees[29]. Ideally it should have a smooth surface
and be free of contamination and etch marks. The tip is usually pre-
pared by an electropolishing technique. Tables on polishing solutions
and conditions for various materials are given by a number of
authors[11,29,30].

In preparing tips for our experiments the method first in-
troduced by Muller[30] had been employed. A General Electric undoped
218 tungsten wire has been used. This tungsten wire is 0.004 inch
diameter and 99.95% purity and is spot-welded to a support filament

before polishing to prevent damage to the tip in subsequent handling.
The wire is then dipped vertically through a thin layer (3-5 mm) of
20% KOH electrolyte floating on carbon tetrachloride. A potential
(3-5 volts A.C.) is applied between the wire and a second electrode
and polishing is continued until the lower part of the wire drops off.
Backpolishing for between 2 and 5 seconds removes deformed material
from the fracture region. Possible surface contamination introduced
during electropolishing does not present a serious problem as it is
removed by field evaporation in the field ion microscope.

After electropolishing, the specimen is examined under an
optical microscope at a magnification of about 500. The end of a
suitable tip should be unresolvable even at this magnification but the
exact radius can only be determined by experiment in the field ion
microscope itself.

5.5 Tip cooling

With helium ions the smallest distances among neighbouring
atoms on a tungsten surface are well resolvable working with liquid
nitrogen temperature as long as tip radius is below about 300 $\overset{\circ}{A}$[24].
The more expensive coolants, liquid hydrogen and liquid helium, have
not been used in our experiments for economical reasons. A consider-
able improvement in resolution is achieved by reducing the pressure
above the nitrogen in the inner dewar thus cooling the liquid nitrogen
to the freezing point of 63°K when a pressure of about 100 torr is
reached.

An ED75 mechanical pump was added to the system to reduce
the working temperature by reducing the pressure above the inner

dewar. The main reason for a further reduction of the working temperature in our experiments is to prevent diffusion of interstitials produced by bombarding the tip with ions of various energy to the surface of the tip thus enabling by controlled field evaporation to locate their true site. The significant improvement in image quality compared to normal liquid nitrogen cooling is an added advantage.

5.6 Photography

For such low image intensities encountered in field ion microscopy an optimum choice of photographic equipment and material is essential. For our experiments a Miranda camera with a Nikkor-S F:1.2, f = 55 mm lens has been used. Stopping down to F:2 facilitates good resolution across the image diameter of about 50 mm. A highly sensitive panchromatic film (Kodak Tri-X-Pan) processed with a highly active developer (Diafine) has been found to give satisfactory results.

As the screen brightness increases with the ion energy, following approximately a $V^{1.1}$ to $V^{1.5}$ law[28], the exposure time decreases accordingly. The exposure times vary from about 15 seconds for tip radii above 600 Å to a about 5 minutes for tip radii below 300 Å.

5.7 Determination of radius of tip specimens

The radius of a tip was either determined by the measurement of field emission current or by counting the number of net rings between two poles of known angular separation in the field ion micrograph.

Employing the first technique the radius of the tip was determined from the Fowler-Nordheim[17] equation:

$$I = a \ V^2 \ exp(- \frac{b\phi^{3/2}}{V}) \tag{5.5}$$

A plot of ln I/V^2 against $1/V$ gives a nearly straight line of slope $-b\phi^{3/2}$. The tip radius which is contained in the constants; $b = 6.8 \cdot 10^7$ $\alpha k \cdot r$ with typical value of $\alpha = 1$ and $k = 5$ was determined by using an average value of 4.5 eV for the work function of the tungsten surface. The radius so obtained is accurate within ±15%.

Using the second technique the average tip radius was determined by multiplying the number of net plane rings from the (011) plane to the center of the (121) plane by 16^{31}. For example, the radius of the tip shown in Figure 3.1 has been calculated to be 570 A° by using the first technique and 650 A° by using the second.

5.8 Electrical equipment

5.8.1 Field ion microscope supplies

The high voltage was provided by a supply capable of giving voltages up to ±30 kV at currents up to 2 mA with a voltage ripple less than 0.01% rms. When working in the field emission mode a negative voltage for the tip is provided by a ±6 kV supply. This supply was also used as a supply for the pulser, so that a pulse up to +6 kV and of 1 to 3.5 msec duration can be superimposed to the high voltage when field evaporation of the tip surface is desired.

Figure 5.2 is a schematic diagram of the electrical supplies for both the FIM and FEM mode. When working in the field ion microscope mode the switches are in the X position. The magnitude of the pulse for field evaporation is set at the 6 kV power supply. When
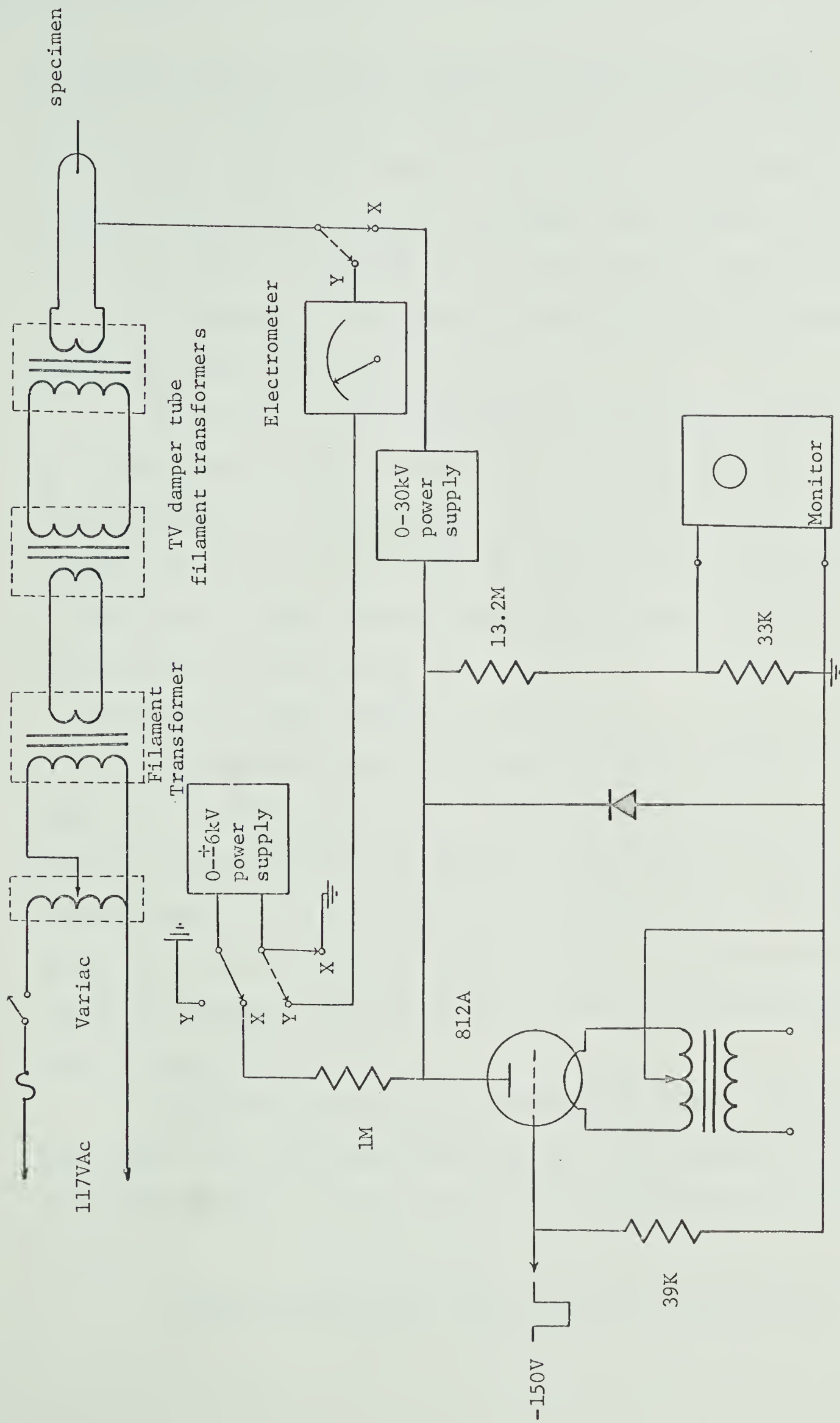
Figure 5.2

cutting-off the 812A tube with a negative voltage from the pulse generator, the preset positive voltage from the ±6 kV power supply is superimposed on the high voltage. The duration of the pulse is determined by the time of the cut-off voltage. When working in the field emission mode the switches are in the Y position. This mode has been used to measure the field emission current which enables evaluation of the radius of the tip.

The tip heat supply was designed to facilitate annealing the specimen while the high voltage is on. Two TV damper tube heater transformers with 7 kV rms insulation each, have been connected back-to-back to the 117 VAc power supply through the filament transformer and a VT1 Ohmite variac. The tip heater has been used successfully without breakdown up to +15 kV.

5.8.2 Ion gun power supplies

A schematic diagram of the ion gun supplies is shown in Figure 5.3. The ionization chamber of the electron beam generator is grounded and potentials that are applied to the electron beam electrodes are with respect to the ionization chamber potential. The potentials applied from the 0.1% stabilized voltage supplies can be monitored with a built-in voltmeter. The electron trap current can also be measured using the same meter.

The ion beam focusing and collimating electrodes are supplied from a 400 V, 0.1% stabilized voltage supply. The potentials are in-dependently variable and the potential of each electrode may be monitored in turn.

A negative potential for the specimen is applied from the
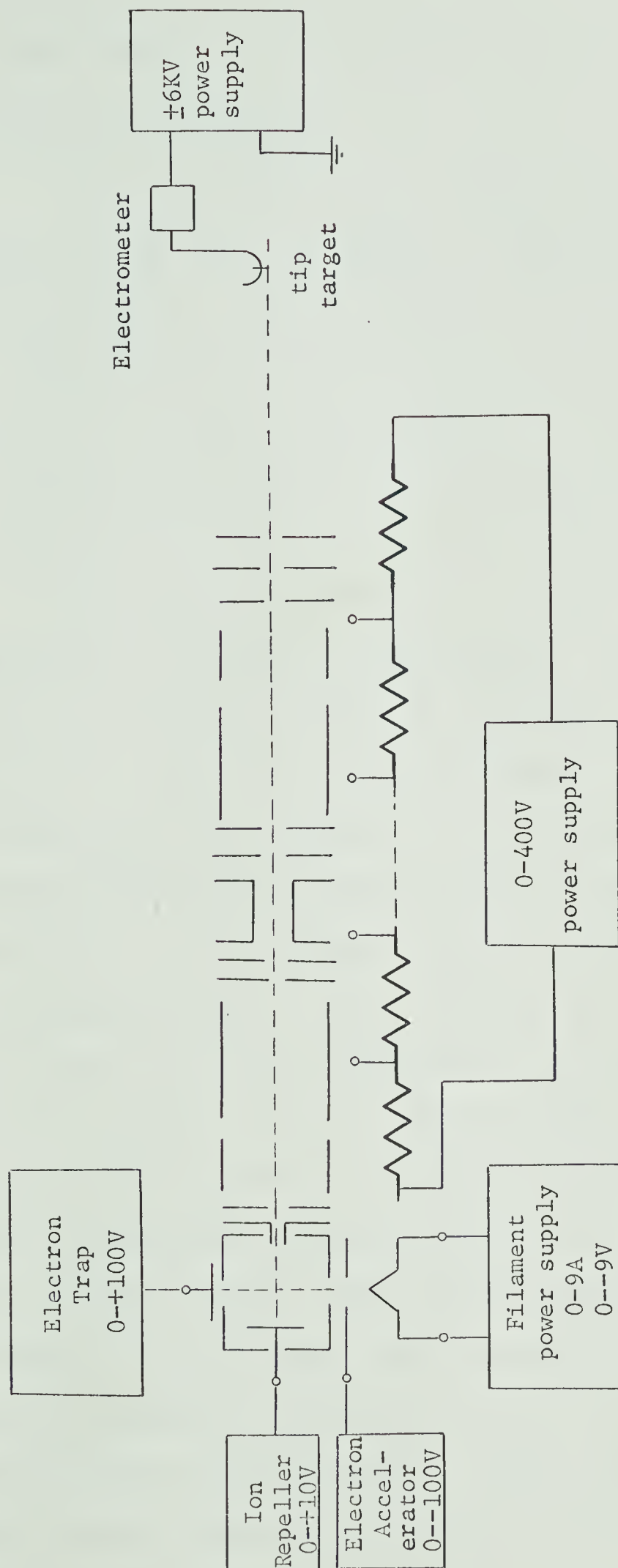
41

Figure 5.3

±6 kV power supply.

5.9 Experimental techniques

The quality of the results obtained were found to be extremely dependent upon the sequence of operations carried out during the experiments. Even at pressures of the order of 10^{-10} torr some contamination of the tip may occur during the various stages of operation if an efficient methodology was not followed. The sequences below describe what is felt to be the optimum procedure that should be and had been followed during a typical experiment.

The background pressure of 1 to 2×10^{-10} torr was routinely achieved after the system had been baked out. The ion gun and sublimation pump filaments were kept on continuously thus preventing gas bursts when in operation. The ion gun filament current was normally set at about 2.25 A and increased to 3.25 A during operation. The sublimation pump filament current is kept at about 30 A and was operated at 50 A before helium or argon was introduced into the system. The specimen was heated to a dull red heat for outgassing before cooling the system. Additional outgassing of the specimen was performed also after the system had been cooled and before an actual experiment. The heating time depends upon the radius of the tip. One must keep in mind that prolonged heating may blunt the tip, thus making it useless for further studies. Since the field ion image is very dim, particularly for small radii, camera focusing is an inevitable problem. During the heating of the specimen therefore, the light shining on the screen was used to focus the camera. Small irregularities of the phosphor coating enable this to be done satisfactorily.

Filling the specimen dewars has of necessity to be carried out slowly. One hour was found desirable since it was found that several times, during the course of rapid cooling, a leak developed in these dewars. The leak usually disappeared upon warming up the system thus precluding its localization. After cooling the system the pressure fell to approximately 6×10^{-11} torr.

The ion pump had been switched off before inert gases were admitted to the system. Exposure of the ion pump to high inert gas pressure of helium or argon, may lead to previously pumped gases being released and consequently contaminating the inert gas. Before helium was admitted to the system the high voltage had been applied to the tip. Helium was expanded into the small volume of the GHP in the line between the valve 5 and 8 (Figure 4.3) from the flask G4. The speed at the main valve is reduced almost to zero by leaving it open only about one quarter to one half of a turn. The leak valve is then opened to allow the imaging gas to flow into the system. This gas is thus pumped continuously and prevents accumulation of any residual gas that may be released from the walls of the system or introduced with the gas from the GHP. Having obtained the field ion image on the screen, the ion gun filament and sublimation pump filament must be turned off to remove excessive light that disturbs the observations. By the process of field evaporation the surface of the tip can be cleaned. A photograph of the image is then taken.

CHAPTER 6

RESULTS AND DISCUSSION

6.1 The effect of the impact of 150 eV energy Ar^+ ions on tungsten

The examination of the specimen in the field ion microscope
prior to bombardment was undertaken to assess the concentration of
defects present in the annealed material. In the subsequent experi-
ments the specimens were irradiated at 60°K temperature and then
warmed up to 78°K. A comparison is possible by taking a micrograph
at each of these steps, i.e., before bombardment, after bombardment
and after subsequent annealing. To avoid ambiguity the same test has
been done for the same nonirradiated specimen, i.e., annealing such a
specimen from 60 to 78°K and then observing for possible interstitial
diffusion or vacancy migration. Such events have not been detected.

Muller observed interstitials to appear on the surface at
a temperature above about 50°K on specimens that had been irradiated
with 20 keV He atoms[12]; on further heating of the specimen in the
temperature range of 85 to 95°K he observed an abundance of inter-
stitials coming out to the surface. Present experiments have been
carried out with solid nitrogen thus the lower temperature was limited
to about 60°K when pumping above liquid nitrogen to solidify it. At
the time when these experiments were made, a heater to warm up the
specimen had not been built into the system, so the temperature lati-
tude was confined between solid and liquid nitrogen. Although the
temperature variation is relatively small, valuable results have been
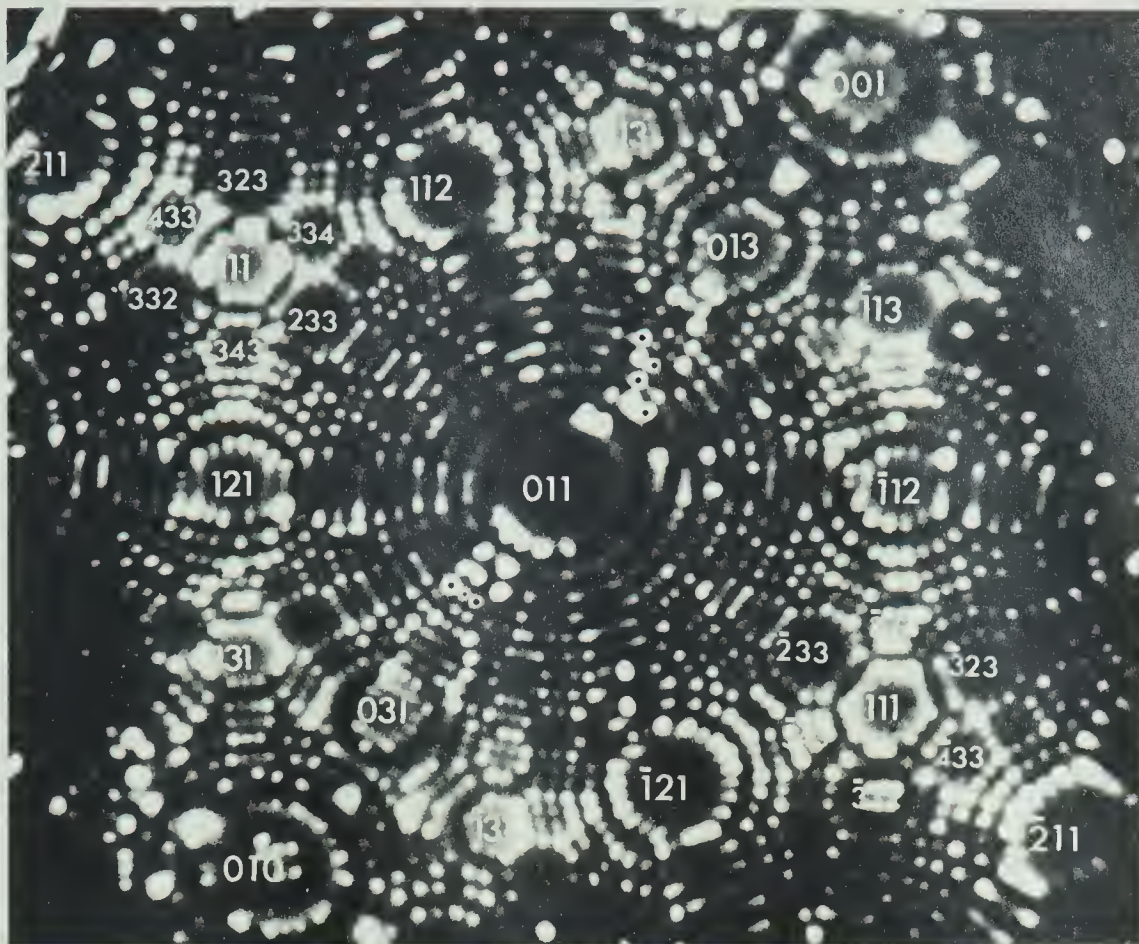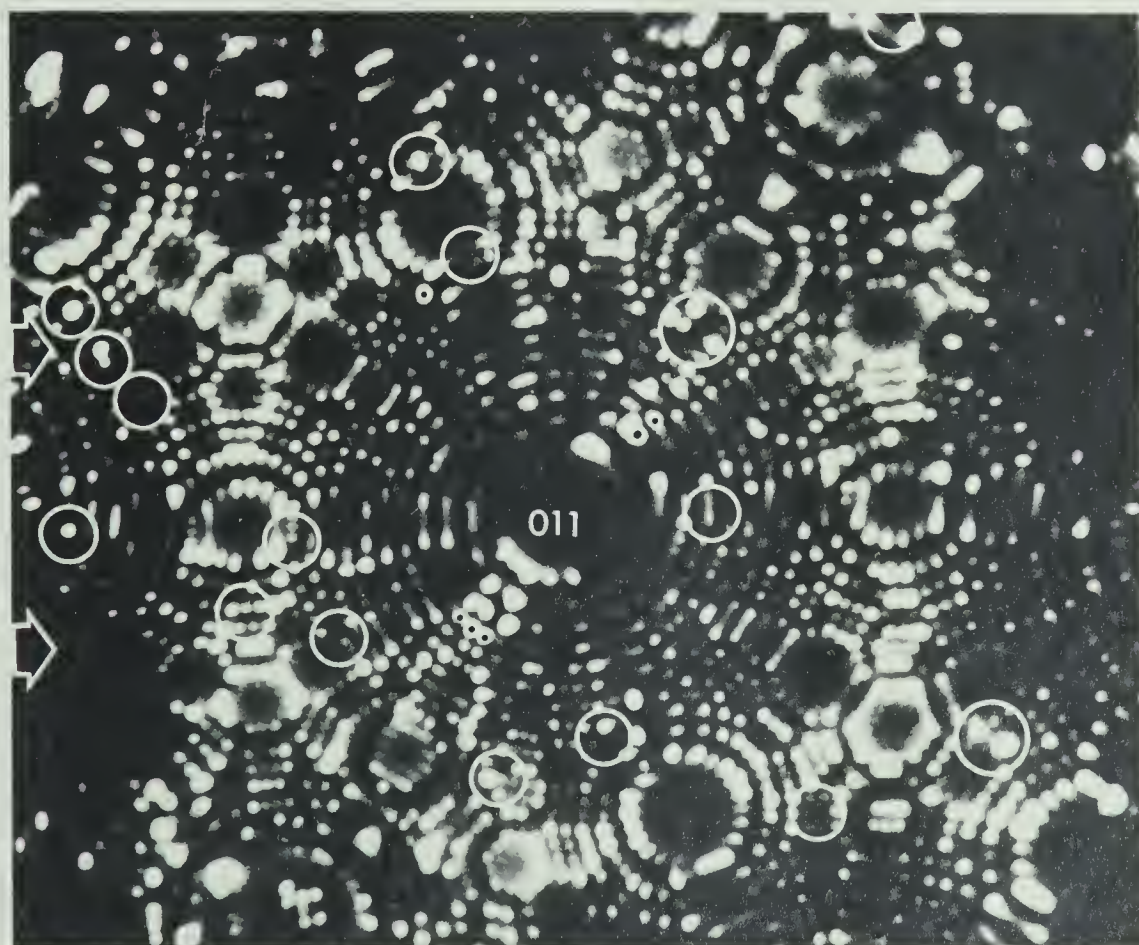
Figure 6.1a

Figure 6.1b

obtained. The heater that has been built into the system in a latter

stage, will enable heating the specimen to an arbitrarily high temp-

erature while the high voltage is applied to the specimen.

Figure 6.1a shows a nearly perfect tungsten tip of approx-

imately 300 A° radius before bombardment. The same surface is shown

in Figure 6.1b after bombardment of 150 eV ions for 45 secs at 60°K.

The direction of incoming ions is shown by arrows. Comparing the two

micrographs the differences were found and encircled on the micrograph

taken after bombardment. In the micrographs that follow, encircled

areas indicate changes that are encountered with respect to the pre-

ceding micrograph. It is readily seen that residual gas contamination,

which may have ocurred in an impure vacuum system during the bombarding

time when the high voltage was off, has not masked the surface thus

allowing immediate inspection of the irradiation induced defects. An

extra 7 bright spots and 11 missing atoms have been found, also the

brightness of at least 10 atoms has changed considerably. Vacancies

are found on the (112), (001), and (013) planes, by the ($\bar{1}$21) plane,

by the (332) plane and between the (121) and the (131) plane. New

bright spots appear on the (112), ($\bar{4}$33), (110), and (031) planes and

by the (332) plane. The brightness of the atoms has changed on the

second, third, fourth, and fifth step of the (011) plane towards the

(013) plane. Similarly, the brightness of three atoms on the third

step of the same plane towards the (031) plane has changed and so has

changed the brightness of the atom on the second step of the (112)

plane. All these are marked by a dot.

There is no doubt that some of the atoms that appear on the

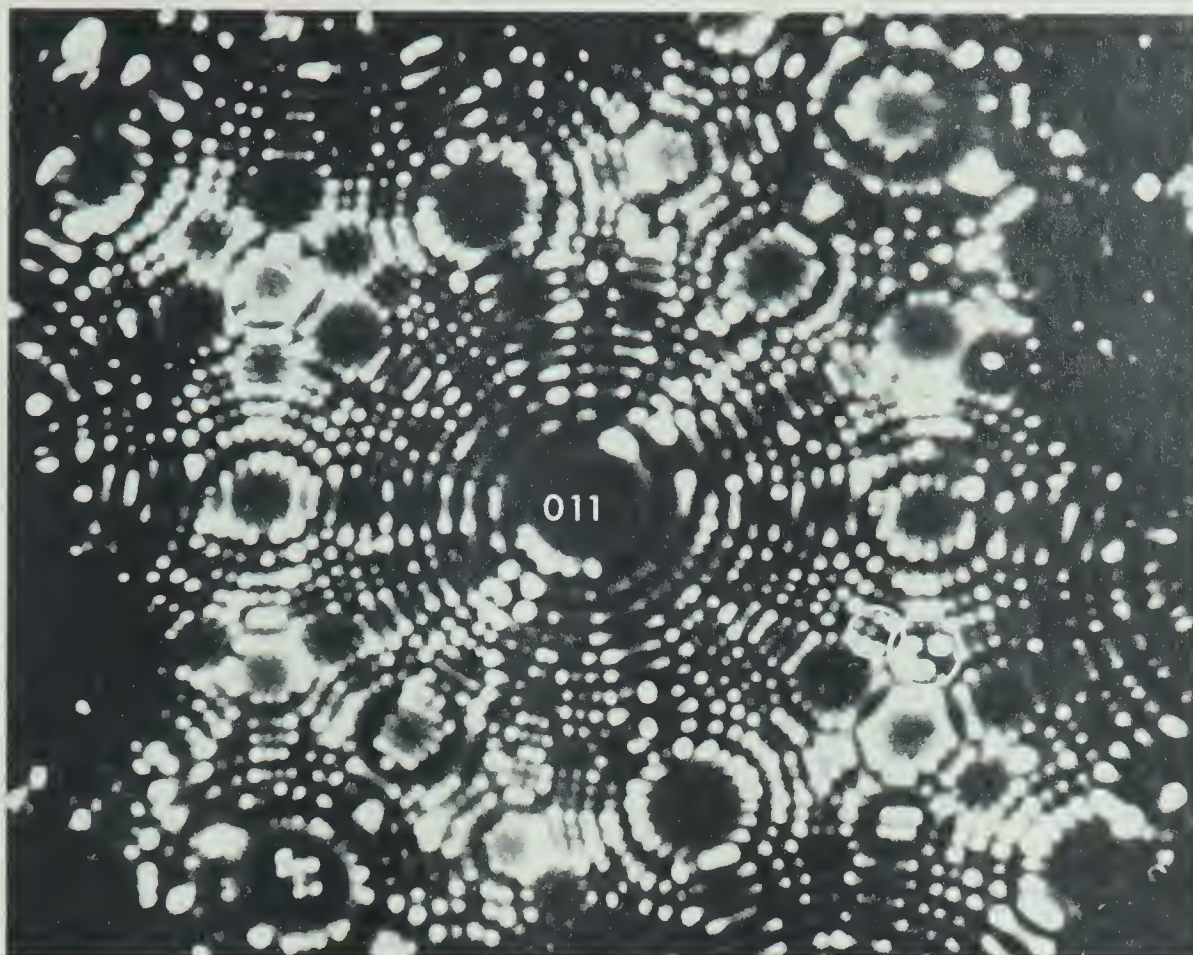surface may be residual gas atoms that were adsorbed during the time
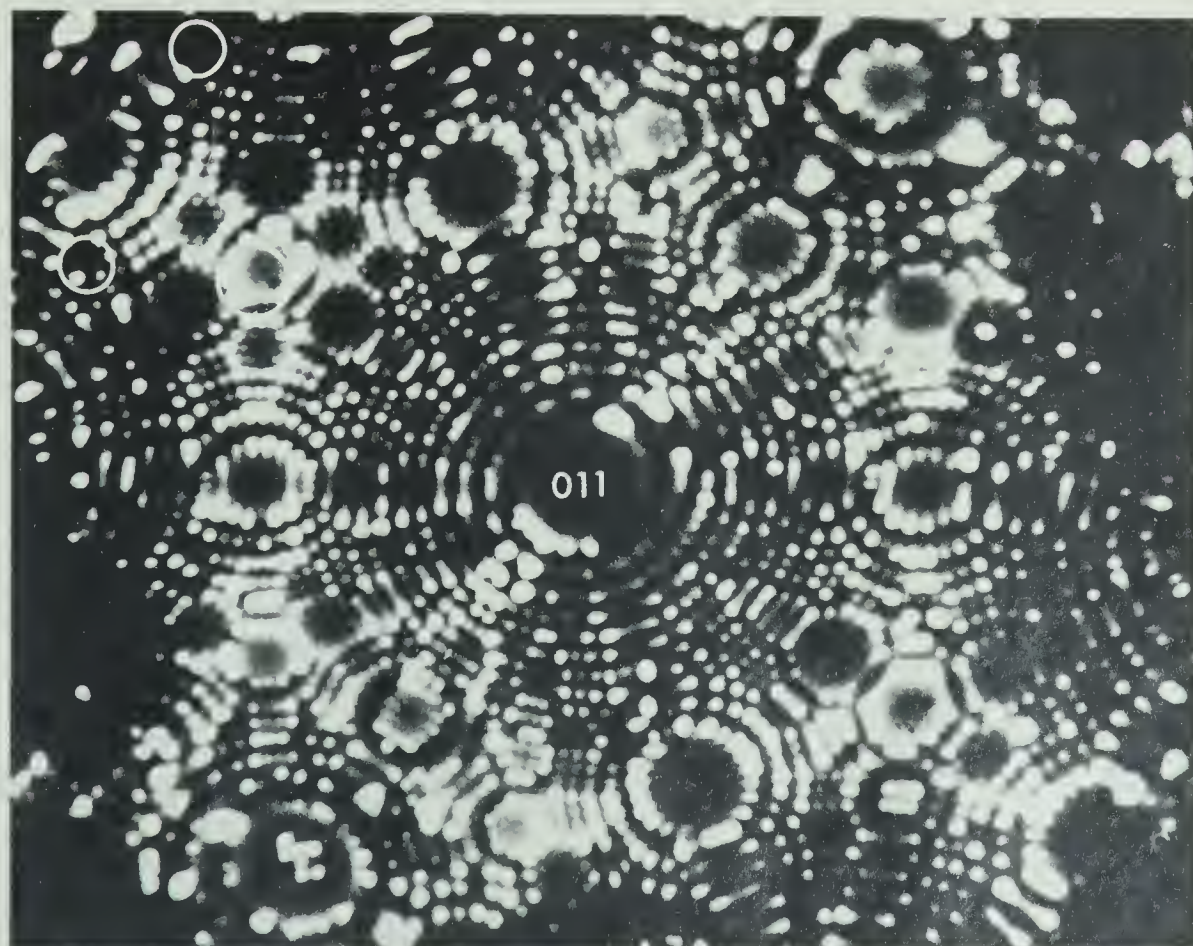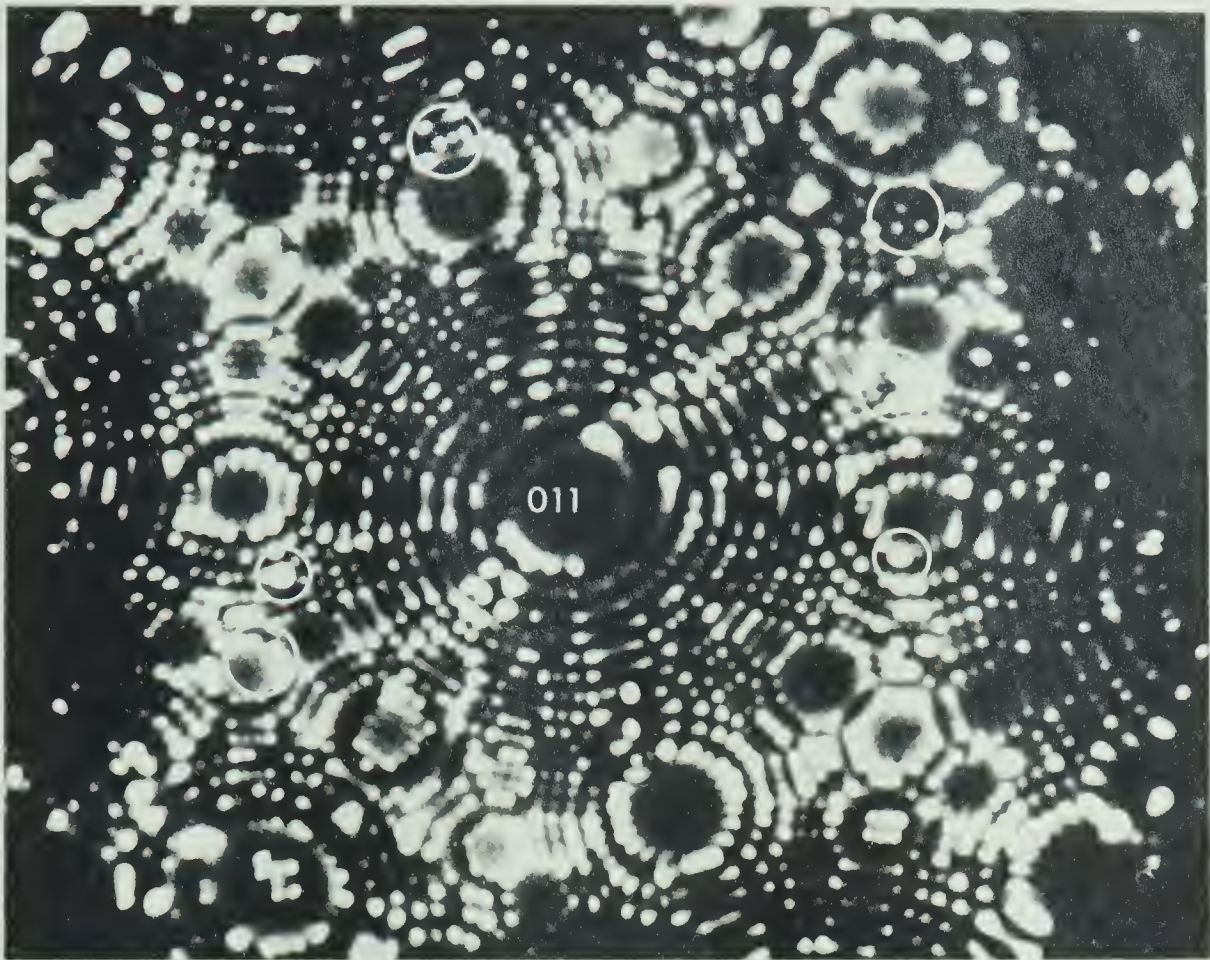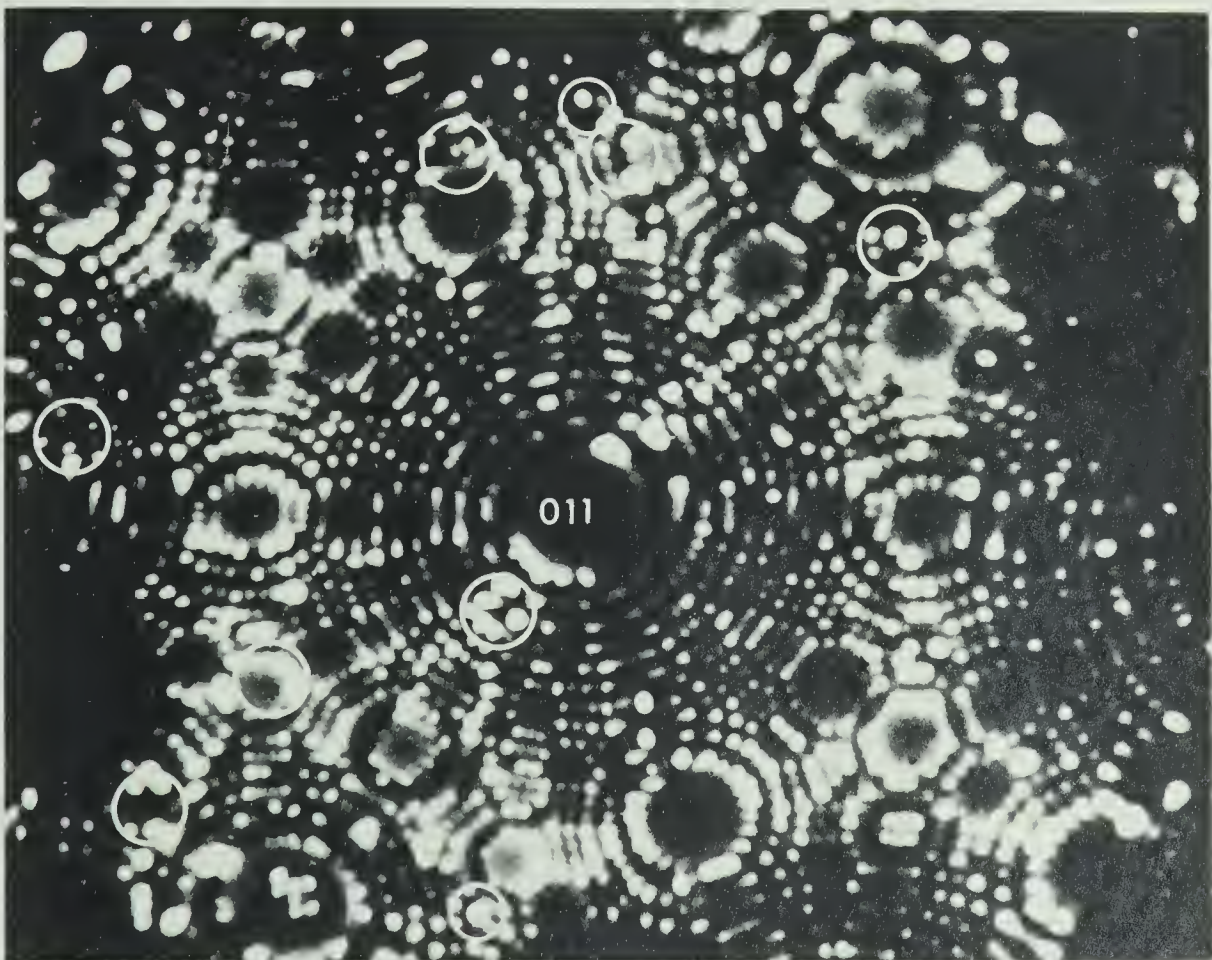
Figure 6.1c

Figure 6.1d

Figure 6.1e

Figure 6.1f

when the specimen voltage was off. Some of the vacancies also may be artifacts that may occur in a variety of situations[32]; in this case caused by being removed together with adsorbed atoms that are removed by field evaporation when the high voltage was turned on again. Considering the next micrographs it can be seen that the irradiation is responsible for many changes on the surface.

Figure 6.1c is a micrograph of the same surface at 60°K a few minutes after the bombardment is over. It can be seen that most of the atoms that had been encountered after bombardment have found a stable site and have not been removed by the field. Three atoms have evaporated as a group on the (334) plane and one atom that has diffused fills a vacant site at the edge of the (111) plane. After warming up the specimen to 78°K (Figure 6.1d) two more changes have occurred on the (111) plane; another interstitial has diffused by the previously diffused atom and at the same time one atom has evaporated from the middle of the plane. Other atoms that have evaporated are encircled on the micrograph. For tungsten at these temperatures the image should be stable since the field-evaporation field is higher than the image field[11]. A probable explanation for the removal of these atoms would be a reduction in the binding energy of these atoms caused by an underlying interstitial atom. As has been seen, the atom that is normally well protected from the field in the middle of the plane is missing only one atom spacing from the atoms that have diffused at the edge of the same plane.

It has been suggested by Sinha and Muller[12,33] that surface relaxation over underlying interstitial atoms (Figure 6.2a) will give

rise to field enhancment over a large region and at the same time
reduce the image force tending to pull the interstitial onto the
surface.

relaxed atoms

(a)

interstitial in
surface site

interstitial

exchange annihilation
of surface

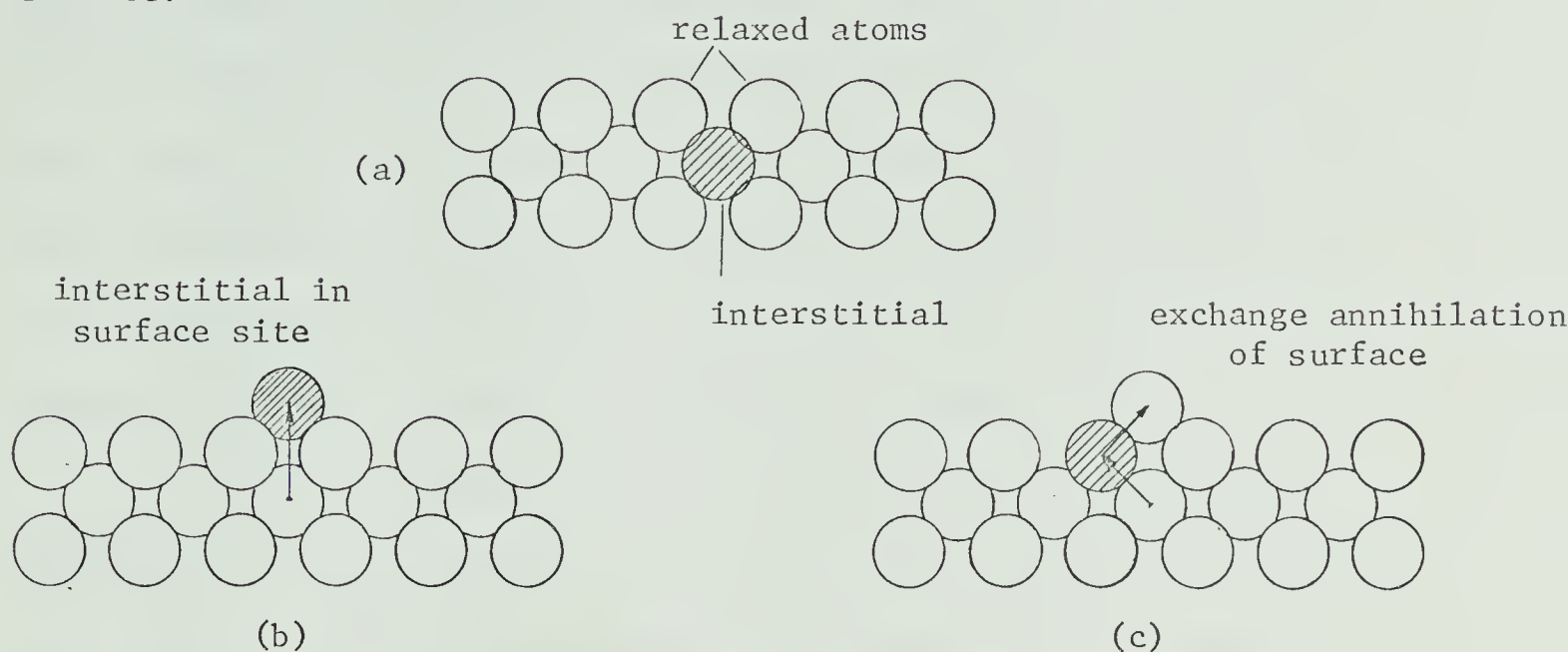(b)   (c)

Figure 6.2

Surface relaxation will also reduce the energy barrier to interstitial
migration enabling the interstitial to move into a stable site either
at the surface (Figure 6.2b) or, more likely by pushing a neighboring
atom to the surface (Figure 6.2c).

While the changes on the (111) plane can be followed and
therefore easily envisaged by this mechanism, the changes in bright-
ness of the previously mentioned atoms may be somewhat difficult. The
mechanism explained above may be responsible for a change in the
brightness of some of the atoms. However, for the atoms that are on
the (011) plane and have undergone change it can be noted that those
that are closer to the ion source have become dimmer. A possible
explanation, then, would be that they might have been knocked-on by
incoming ions, replaced by argon atoms, and as a result affecting the
field ionization distribution above their neighbours that now get more

imaging gas supply and as a result become brighter. Though a combination of both mentioned mechanisms is not excluded, i.e. those atoms that are presumed to have been knocked-on, might have been replaced by interstitials that were burried and tend to fill vacant sites. This would be similar to the event that has been explained and took place on the (111) plane after annealing the specimen (Figure 6.1d) or to the one that has occurred on the (131) plane (Figure 6.1e and Figure 6.1f) and for which the description is given below.

The micrographs in Figures 6.1e and 6.1f represent the surface of the same specimen a few minutes after warming the specimen up. New interstitials and vacancies are found (encircled areas). Of these a very interesting observation is the change that has occurred on the (131) plane. Here, one atom has evaporated from the edge of the plane leaving a vacancy behind (Figure 6.1e). On the next micrograph (Figure 6.1f) the vacant site is filled with an atom and at the same time a new vacancy appears in the middle of the plane. This gives another point, and that is: not all vacancies or interstitials are detectable since an underlying interstitial that is responsible for the field evaporated atom fills its site.

It has been suggested by Brandon[33] that vacant lattice sites on close-packed planes lower the binding energy of neighbouring atoms and give rise to preferential removal of these atoms at the surface. Because preferential removal of one atom results in both local field enhancement and a reduction in the binding energy of neighbouring atoms, the atoms around a vacant lattice site tend to evaporate as a group. In the present experiment such an event is seen to have

occurred after annealing the specimen on the $(\bar{3}\bar{3}4)$ plane (Figure 6.1c) and on the (113) plane (Figure 6.1f).

6.2 The effect of the impact of 300 eV energy Ar^{+} ions on tungsten

This specimen, of approximately 340 A° was irradiated with 300 eV energy Ar^{+} ions at a temperature of 60°K. The ion current was 1.2×10^{-9} A and bombardment time 2 minutes.

Figure 6.3a shows a clean surface of the tip prepared by heating and subsequent field evaporation. The same surface is shown in figure 6.3b after bombardment. Though the background pressure was less than 1×10^{-10} torr and the high voltage was off for only 3 minutes some contamination still could have occurred. There have been detected about 23 new bright spots and 14 missing atoms. The damage is found across the whole area of the specimen and as at 150 eV energy, the density of surface damage is greater on the side of the tip towards the ion source.

The image voltage for the tip after bombardment was kept 500 V lower than the "best image voltage" (Figure 6.3b). As the voltage was gradually increased to the "best image voltage" figure 6.3c a number of bright dots were seen to come out from the interior of the tip. A few vacancies were also produced in this process. The changes with respect to the preceding micrograph are encircled. The diffusion of interstitials to the surface during the increase at the tip voltage towards the "best image voltage" was observed by Muller at much lower temperature $(21°K)$ [12]. He attributes these results to the effect of the field stress on the activation of interstitial diffusivity. The arrival of new atoms onto the surface upon increasing voltage to
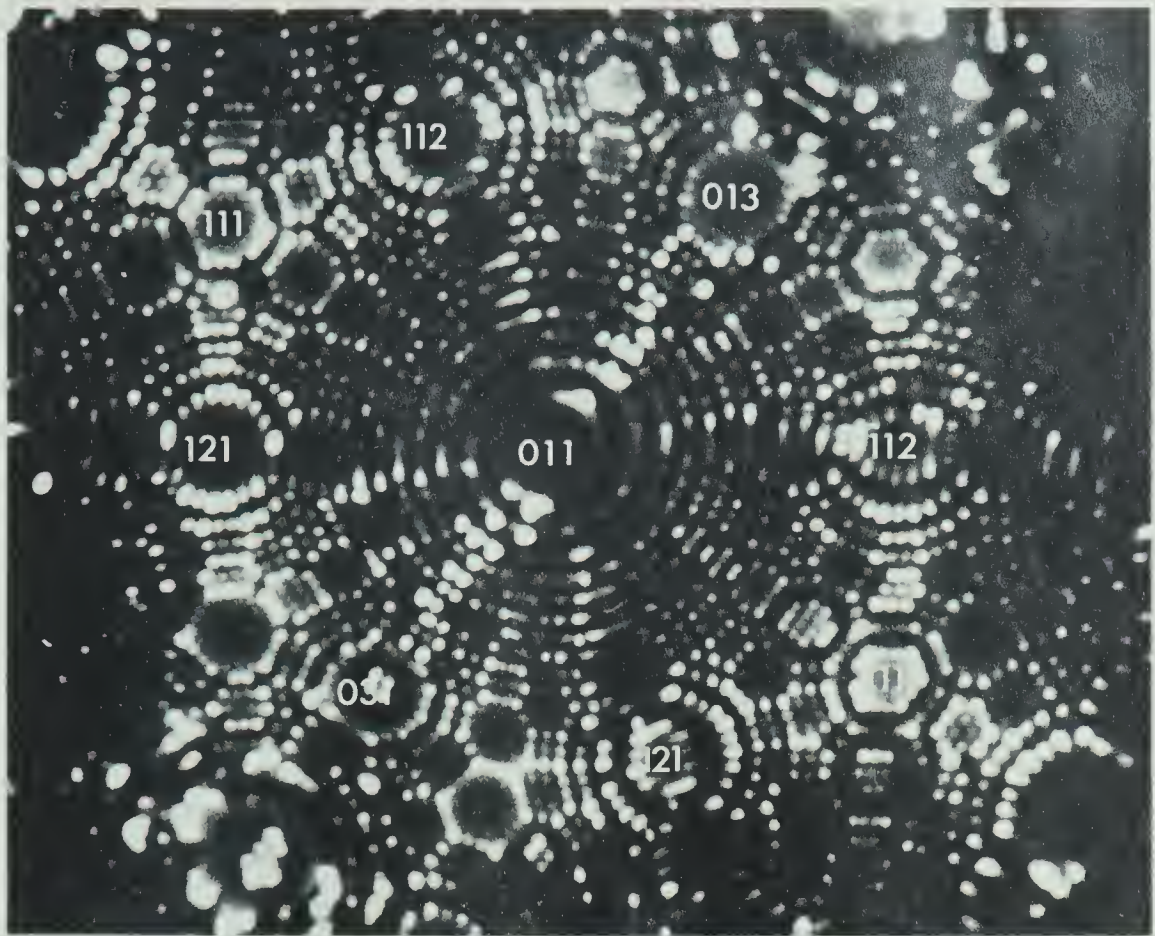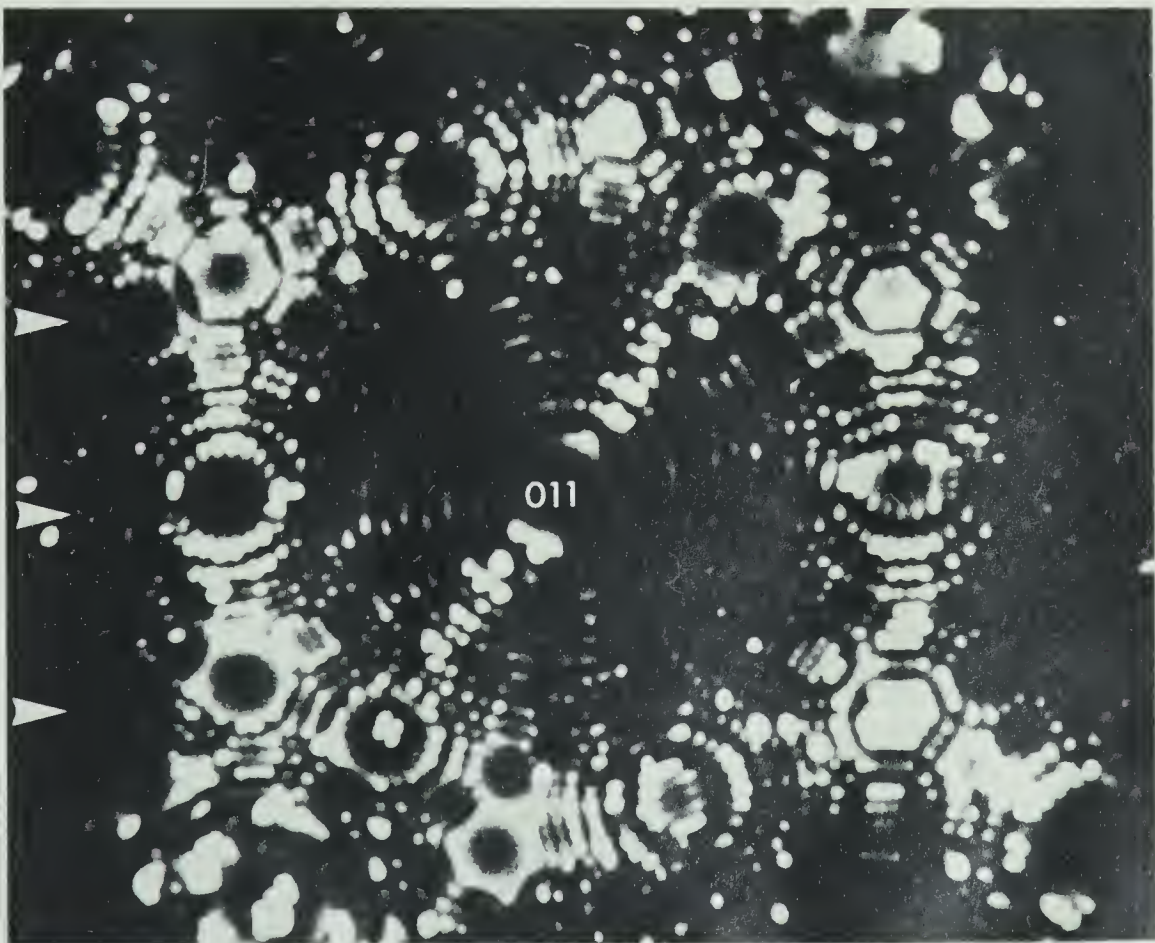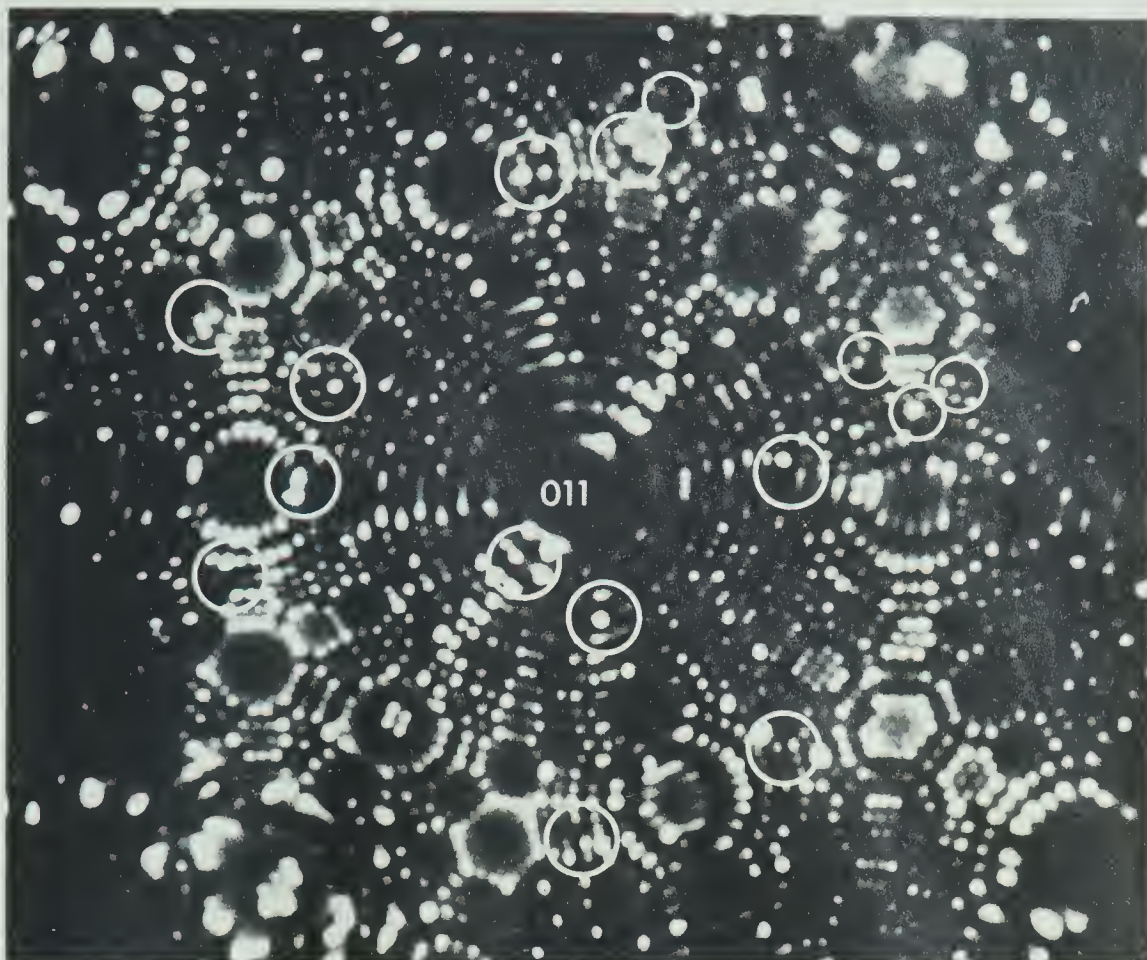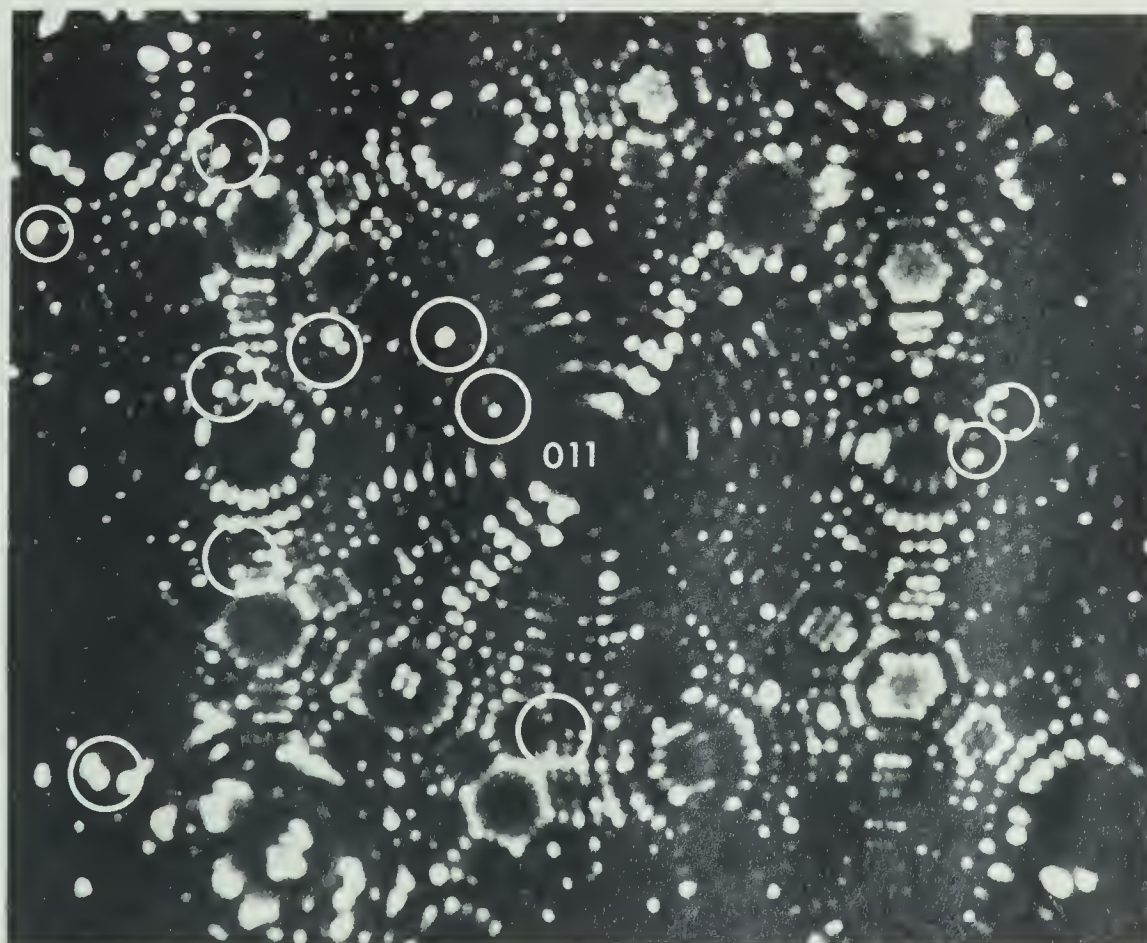
Figure 6.3a

Figure 6.3b

Figure 6.3c

Figure 6.3d

8000 V (best image voltage) at the temperature of 60°K may also be assisted by the field stress that effects the activation of interstitial diffusivity. After the specimen had been heated to 78°K, displaced atoms appeared on the surface and a few vacancies were produced. These changes are encircled on Figure 6.3d. The change that the surface has undergone upon irradiation and subsequent annealing does not differ much from that irradiated by 150 eV energy Ar^+ ions. The micrographs in Figure 6.1b and in Figure 6.3b show tungsten surfaces after bombardment. Since the high voltage was turned off during the bombardment time, some of the changes found on these micrographs may be attributed to adsorbed gas contaminants. However, the changes that follow with the high voltage on all the time (Figures 6.1c to 6.1f, and 6.3c and 6.3d) are due to the irradiation induced defects on the surface and the bulk of the tungsten. Counting only these changes it is found that the number of changes that have occurred on the side of the tip towards the ion beam is two times greater than on the opposite side of the beam.

The chemical nature of the bright spots appearing upon bombardment and subsequent annealing may be found by using the atom-probe FIM^{34}, a modification of the FIM that enables identification of the atomic species associated with individual image dots. By using this technique the mechanism of formation of underlying and surface interstitials may be more exactly established. This technique would allow distinction between displaced atoms to impurity or beam particles.

6.3 The effect of the impact of 400 eV energy Ar^+ ions
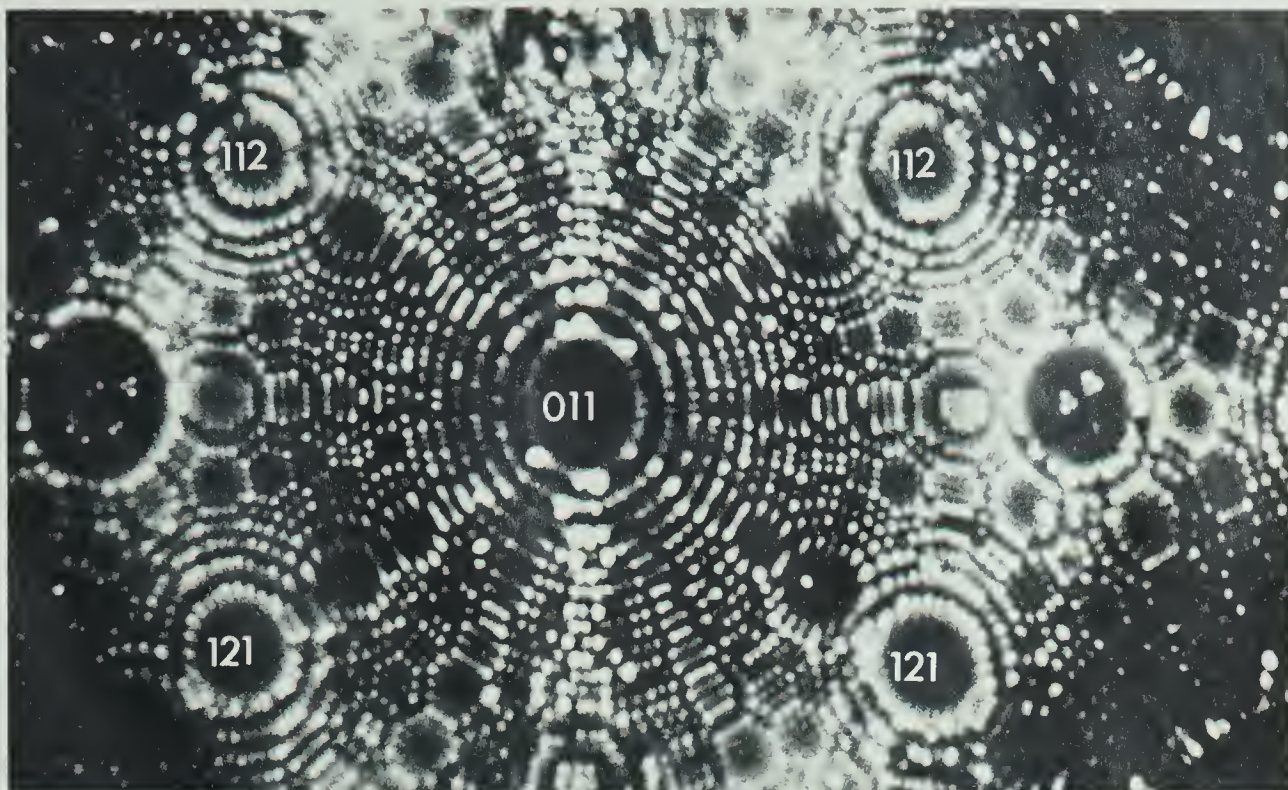
The surface of the specimen that had been irradiated with

Figure 6.4a
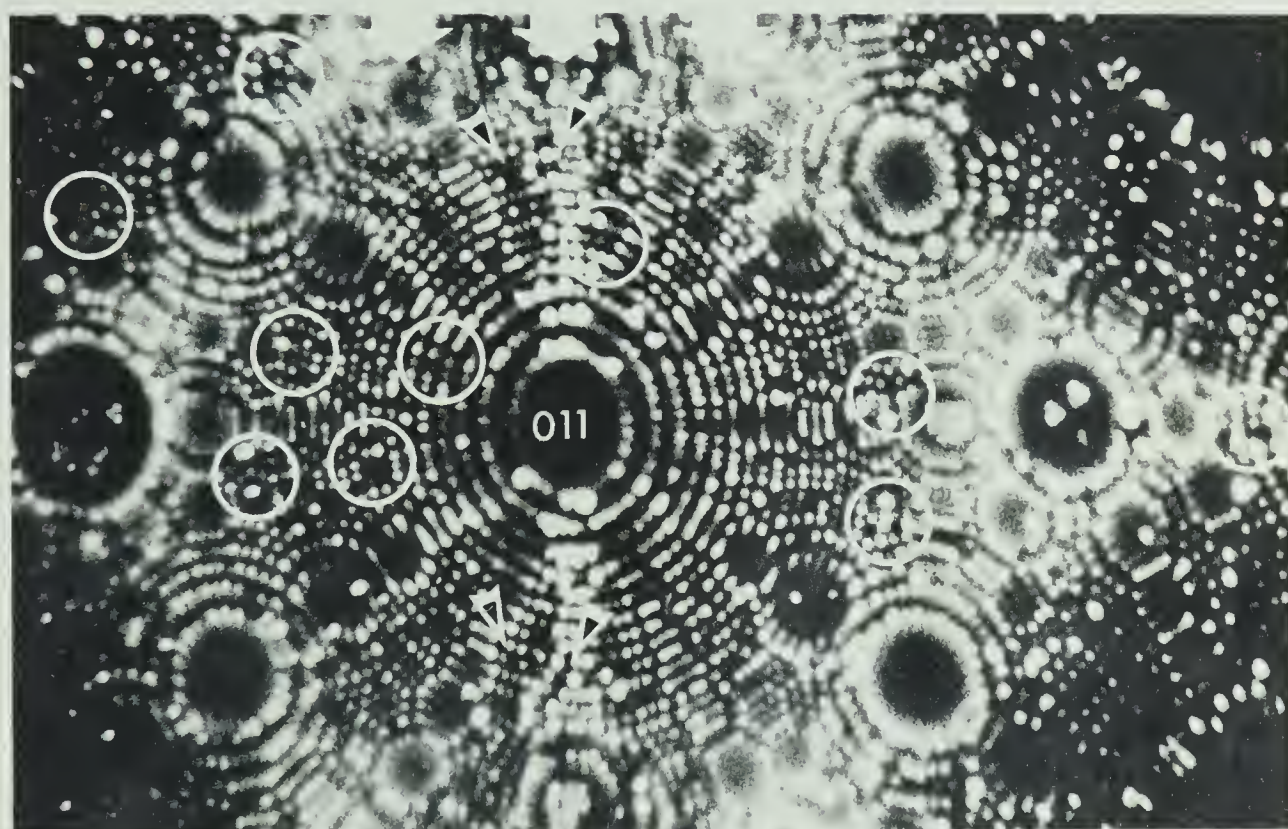

Figure 6.4b

400 eV energy Ar$^+$ ions at 60°K temperature is shown in Figure 6.4a.

The ion current was 1.4×10^{-9} A, the bombardment time 90 secs, and the

specimen without the high voltage for 4 minutes. The specimen has

been irradiated in the direction of the [100]-zone. The direction of

the incident particles is indicated by the broad arrows. The same

surface after bombardment is shown in Figure 6.4b. The encircled

areas indicate some of the damage introduced by the bombardment. Four

thin arrows in Figure 6.4b indicate an interesting event that took

place on the tenth atomic layer below the top (011) plane of the

specimen. On the side of the tenth net plane ring towards the ion

beam there are five surface vacancies, and on the opposite side, in

the direction of [100]-zone, there are two atoms missing. These

vacancies, it is believed, are created by an assisted focusing event

in the [100] direction. The number of atoms involved in the focusing

sequence is about 30. Assuming the hard sphere condition, Nelson[5]

evaluates a focusing energy for the [100] focusing sequence in tungsten.

According to his calculations a sequence starting at E_f^{100} = 200 eV

will make approximately 20 collisions before attenuation. At this

energy successive collisions occurring before 0 (Figure 6.5), con-

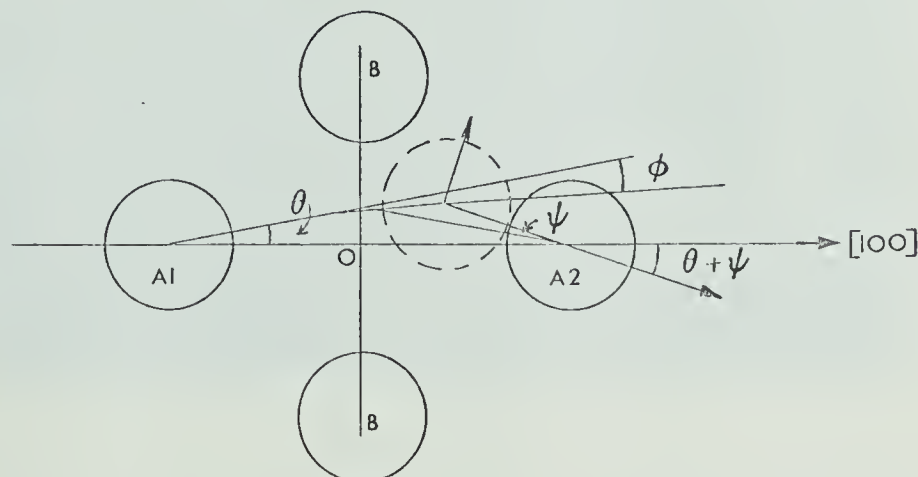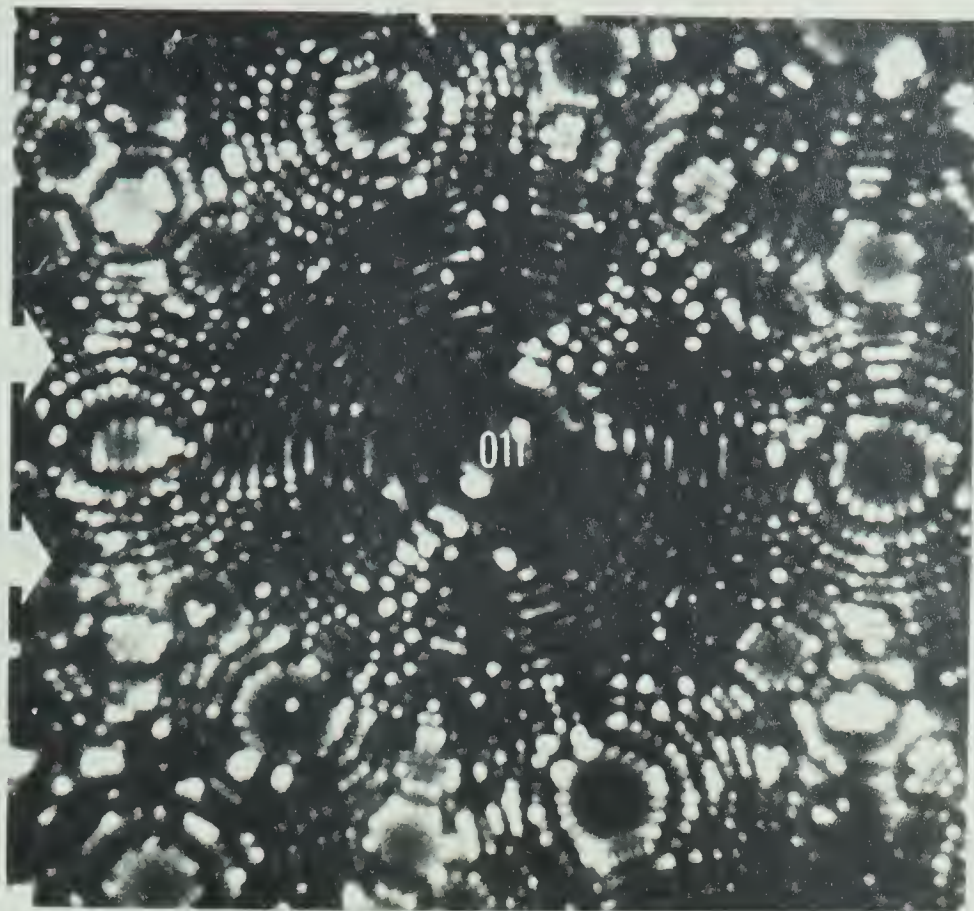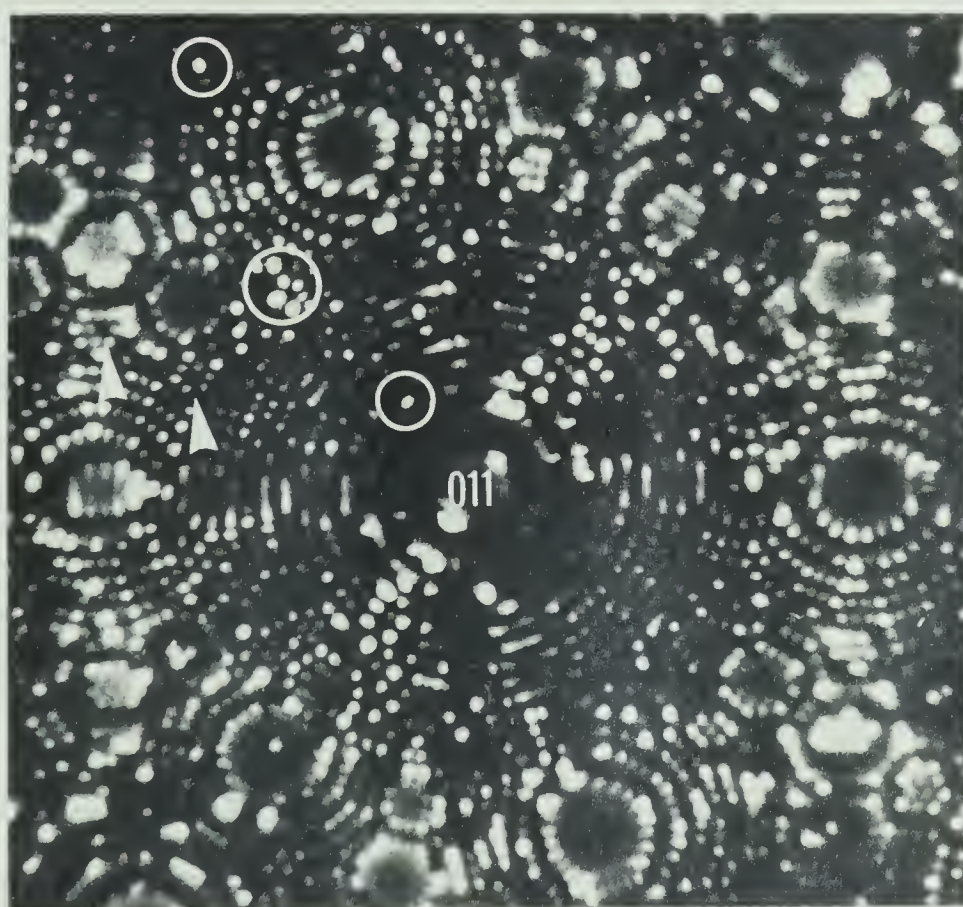sequently only transfer momentum.

Figure 6.5

Figure 6.6a

Figure 6.6b

Because of the potential maximum at the focusing ring, sequences which propagate with successive collisions occurring beyond 0 will be of a replacement nature. The focusing event found on the previous micrograph is initiated with 400 eV energy that corresponds to 260 eV transferred energy. This energy would be, therefore, sufficient to promote a focusing event assuming a head-on collision.

Figures 6.6a and 6.6b show a tungsten surface upon irradiation of 400 eV energy. Figure 6.6a is the specimen surface after field evaporation of a few atomic layers and Figure 6.6b after subsequent annealing to 78°K temperature. Six interstitials have come out at the (011) plane (encircled area). One atom has diffused on the (011) plane and another one on the (101) plane. Two vacancies have been created in the annealing process, and are indicated by arrows. The cluster of interstitials represents a damaged area which had been created in the interior of the target. After a few atomic layers had been removed by field evaporation, these interstitials, being one or two atomic layers below the surface, diffused to the surface upon annealing.

6.4 The effect of the impact of 450 eV energy Ar^+ ions

A tungsten tip of an average radius of 600 A° has been irradiated with 450 eV Ar^+ ions, that would correspond to an average knock-on of 300 eV transferred to the primarily hit tungsten atom. The ion current was 1×10^{-9} A, the bombardment time 120 secs, and the specimen without the high voltage for 5 minutes.

Figure 6.7a is part of the specimen surface before, and Figure 6.7b the same surface area after bombardment. Extensive damage
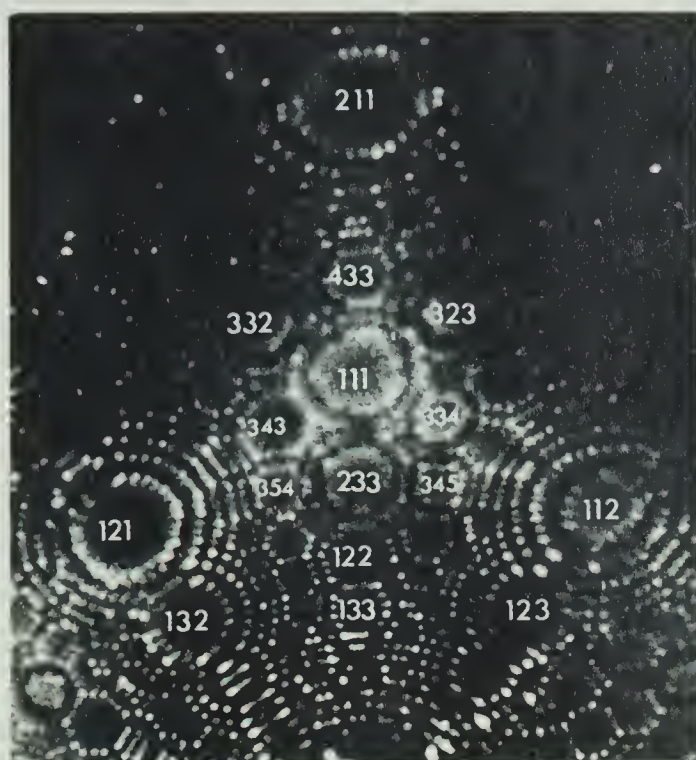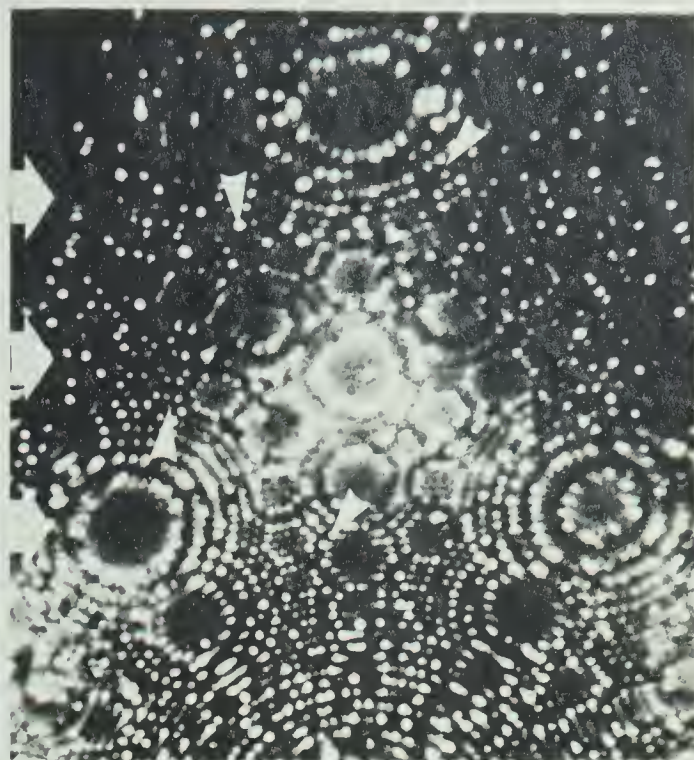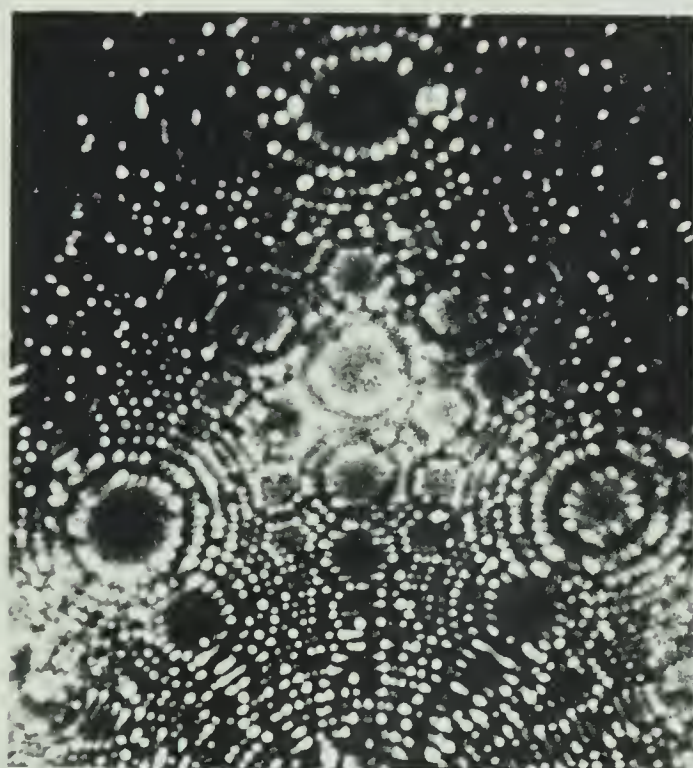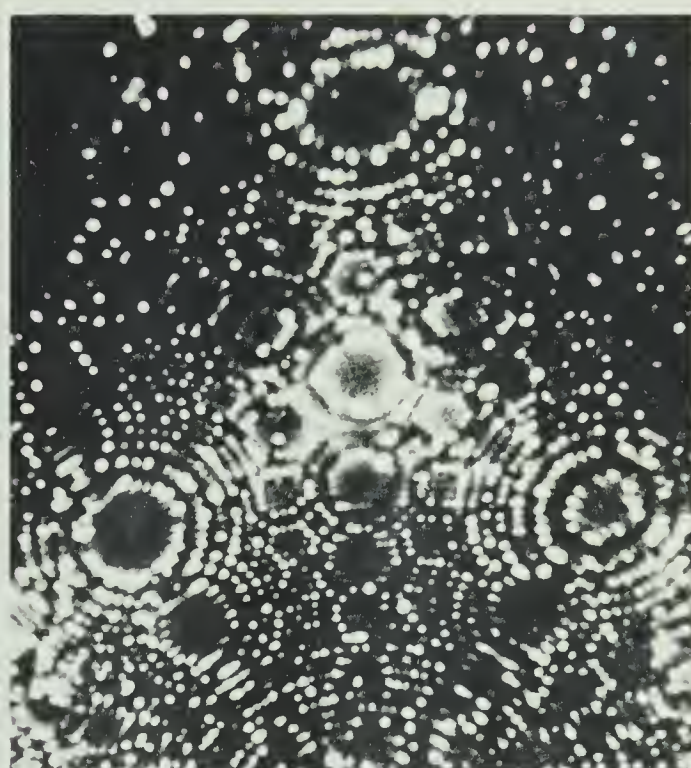
Figure 6.7a

Figure 6.7b

Figure 6.7c

Figure 6.7d

has been induced across the whole area of the specimen. Besides num-
erous interstitials and vacancies a large number of vacancy clusters
have been created. Some of the vacancies may be located in the middle
of net planes, for example on the (354) and (133) planes. The vacancy
clusters consist of two up to ten vacancies. Some of the vacancy
clusters are indicated by arrows. One vacancy cluster, consisting of
about 10 vacancies that extends to the (122) plane can be easily
located and is also indicated by an arrow.

Figure 6.7c shows the same surface area after warming the
specimen up to 78°K temperature. An easily detected change is an
interstitial that has come out on the (343) plane. Similar changes
can be observed across the whole area of the tip.

The same surface area of the specimen is shown in Figure 6.7d
after partial field evaporation that removed some of the protruding
atoms. The image is somewhat improved due to the better chosen high
voltage[11]. The vacancies and vacancy clusters are better identified
on this micrograph. There are some artifacts i.e., dead spots on the
phosphor screen (for instance on the (343) plane), but they are easily
distinguished from 'real' vacancies. One atom has diffused on the
(433) plane, and one on the (233) plane among other changes that may
be identified by comparing the two micrographs (Figures 6.7c and 6.7d).

A continued field evaporation of subsequent atomic layers
makes it possible to observe the damage in the tip interior. To esti-
mate the depth of the irradiation induced damage, a long sequence of
micrographs were taken from the irradiated specimens with 150, 200,
250 and 300 eV energy, with small evaporations between each image.

This, however, has not brought expected results; one of the reasons was that as the field was raised many of the bright spots disappeared under the increased surface stress, and the nature of the remaining bright spots without a FIM atom probe would be difficult to specify. As has been seen in the energy range up to 300 eV only point defects have been observed, while larger defects have been detected on the specimens bombarded with 400 and 450 eV energy. Unfortunately a continued field evaporation for these specimens was not performed thus any estimation of the depth of the damage is not possible.

CHAPTER 7

CONCLUSIONS

7.1 The microscope facilities

The capabilities of the UHV field ion microscope system

that has been constructed, are well demonstrated with the results

obtained. The background pressure in the range of 10^{-11} torr was

achieved after the system had been baked out and when all dewars of

the system were filled with liquid nitrogen. The contamination of

the specimen with residual gases, therefore, presents no problem if

an investigation of the surface is to be carried out with the high

voltage off, providing the time the specimen is without high voltage

is not long.

A controlled field evaporation is possible by using the

pulser and has been used satisfactorily throughout the course of

this work. This controlled field evaporation did not enable an est-

imation of the depth of the induced point defects, such as inter-

stitials and vacancies, to be made, as has been explained. However,

when encountering larger defects one could apply this technique to

determine the extent of the damage in the interior. The image is very

dim and often even larger defects may escape direct observation. It

is recommended, therefore, to use this facility each time when similar

experiments are carried out thus exhausting all available possibilities.

The tip heater that has been built into the system enables

annealing the specimen from the temperature of the coolant to the

desired high temperature. The tip heater may be operated with the high voltage applied to the specimen, thus precluding contamination during the annealing process. It should be noted that increasing the temperature of the tip reduces the evaporation field, therefore the high voltage should be reduced if the surface is to remain atomically identical.

7.2 Results

Bombarding the tungsten surface with 150, 300, 400 and 450 eV energy Ar^+ ions, various types of damage on the surface have been observed. These are: interstitials, vacancies, and their clusters.

The defect density is higher on the side of the tips towards the ion source in the energy range the experiments were carried out. This is the opposite result of Strayer's findings[15].

Only point defects have been observed on the specimens irradiated with up to 300 eV Ar^+ ions, while clusters have been found on the specimens irradiated with higher energy ions. The degree of the damage increases with higher energies.

It is suggested that a focusing sequence is responsible for causing vacancies found on the opposite sides of the (011) plane (Figure 6.4b) after the tip had been irradiated with 400 eV energy Ar^+ ions in the direction of the [100]-zone.

There is considerable damage induced in the interior of the tungsten specimens irradiated with Ar^+ ions. The atoms displaced inside the volume of the tungsten tips diffuse to the surface during annealing.

Vacancies have been created in the annealing process. In their neighbourhood new interstitials have been observed to have diffused onto the surface so supporting the idea that an underlying interstitial that tends to emerge at the surface is responsible for such an event.

7.3 Suggestions for further work

The system that has been designed may be used in investigating the interactions of energetic particles of various masses and energies with surfaces of a number of different materials that are accessible to field ion microscopy. The low background pressure of the system, may allow the application of imaging gases with lower ionization potentials thus enabling imaging of materials that have lower field-evaporation fields, such as gold, iron and others.

In extending the work that has been presented, by using ions of various species (He, Ne, Kr, Xe), one might find some difference in the damage pattern because of the different mass and penetration of the incident particles. Further, it would be desirable to work with lower temperatures, which would necessitate the use of liquid hydrogen or liquid helium, thus freezing displaced atoms in the interior of the material and by controllable annealing to follow changes that could occur on the surface of the specimen. For this purpose a temperature monitor should be devised that would enable monitoring the temperature. Among the advantages of using liquid hydrogen or liquid helium would be: better resolution, higher brightness, and reduced background pressure[11,24,29].

REFERENCES

1. Damask, A.C. and Dienes, G.J., Point Defects in Metals (Gordon and Breach Science Publishers, New York, 1963).

2. Carter, G. and Colligon, J.S., Ion Bombardment of Solids (American Elsevier Publishing Company, New York, 1968).

3. Chadderton, L.T., Radiation Damage in Crystals (Methuen's, London, 1965).

4. Muller, E.W., Z. Phys. 131, p. 136 (1951).

5. Nelson, R.S., Phil. Mag. 8, p. 693 (1963).

6. Kornelsen, E.V., Bulletin N.R.C. of Canada, 11, p. 42 (1961).

7. Kornelsen, E.V. and Sinha, M.K., J. Appl. Phys. 39, p. 4546 (1968).

7a. Kornelsen, E.V. and Sinha, M.K., J. Appl. Phys. 40, p. 2888 (1969).

8. Kornelsen, E.V., Brown, F., Davies, J.A., Domeij, B., and Piercy, G.R., Phys. Rev. 136A, p. 849 (1964).

9. Navinsek, B. and Carter, G., Can. J. Phys. 46, p. 719 (1968).

10. Lawson, R.P.W. and Carter, G., Vacuum 18, p. 205 (1968).

11. Muller, E.W., Advanc. Electron. Electron Phys. 13, p. 83 (1960).

12. Muller, E.W., J. Appl. Phys. 35, p. 1256 (1964).

13. Brandon, D.G., Southon, M.J. and Ralph, B.J., Phys. Soc. Japan 18, Sup. II, p. 324 (1962).

14. Muller, E.W., Surface Science 2, p. 484 (1964).

15. Muller, E.W. and Tsong, T.T., Field Ion Microscopy (American Elsevier Publishing Company, New York, 1969), Chapter 7.

16. Petroff, P. and Washburn, J., Rev. Sci. Instr. 39, p. 317 (1968).

17. Gomer, R., Field Emission and Field Ionization (University

    Press, Harward, 1961).

18. Bohm, D., Quantum Theory (Prentice Hall, New York, 1951).

19. Messiah, A., Quantum Mechanics (Interscience Publishers,

    New York, 1962).

20. Muller, E.W. and Bahadur, K., Phys. Rev. 102, p. 624 (1956).

21. Tsong, T.T. and Muller, E.W., J. Chem. Phys. 41, p. 3279 (1964).

22. Southon, M.J. and Brandon, D.G., Phil. Mag. 8, p. 579 (1963).

23. Muller, E.W., Phys. Rev. 102, p. 618 (1956).

24. Muller, E.W. and Tsong, T.T., Field Ion Microscopy, Chapter 2.

25. Brandon, D.G., Brit. J. Appl. Phys. 14, p. 474 (1963).

26. Hagstrum, H.D., Rev. Sci. Instr. 24, p. 1122 (1953).

27. Gomer, R., Rev. Sci. Instr. 24, p. 993 (1953).

28. Muller, E.W. and Tsong, T.T., Field Ion Microscopy, Chapter 5.

29. Brandon, D.G., In High-temperature High-Resolution Metallography

    (Gordon and Breach Science Publishers, New York, 1967) p. 1.

30. Muller, E.W. and Tsong, T.T., Field Ion Microscopy, Chapter 4.

31. Muller, E.W. and Tsong, T.T., Field Ion Microscopy, Chapter 6.

32. Muller, E.W., In Field Ion Microscopy (Plenum Press, New York,

    1968), Chapter 6.

33. Brandon, D.G., in Field Ion Microscopy (Plenum Press, New York,

    1968), Chapter 3.

34. Muller, E.W., Panitz, J.A., and McLane, S.B., Rev. Sci. Instr.

    39, p. 83 (1968).